Vector Zonal Operations for Spatiotemporal Analysis

BY

Tingting Xu

Submitted to the graduate degree program in
the Department of Geography of the University of Kansas
in partial fulfillment of the requirements for the degree of

Master's of Arts

____Li, Xingong_____
Chairperson*

__Egbert, Stephen_____

___Slocum, Terry_____

_____

_____

Date Defended: ___09/16/2009_____

The Thesis Committee for Tingting Xu certifies
that this is the approved Version of the following thesis:

Vector Zonal Operations for Spatiotemporal Analysis

Committee:

____Li, Xingong_____
Chairperson*

__Egbert, Stephen_____

__Slocum, Terry_____

_____

_____

Date approved: ___09/16/2009____

Table of Contents

Abstract: Cartographic modeling (also known as map algebra) is a powerful set of operations for manipulating raster geographic data. Zonal operations are one type of cartographic modeling operations where the spatial scopes of the operations are defines by zones. The conventional zonal operations only work with raster data and lack the capability of performing spatiotemporal analysis. This research developed zonal operations for spatiotemporal analysis where spatiotemporal zones can be defined in the vector data model. The zonal operations were used to extract watershed hourly or daily precipitation for use in non-point source pollution models and to explore the effects of antecedent precipitation on water quality samples. The case studies demonstrated the usefulness of the operations. A software tool, NexTool was also developed to process and build NEXRDA precipitation database, which was used in the case studies.

Key words: GIS, cartographic modeling, zonal operation, spatiotemporal analysis, NEXRAD

Chapter 1. Introduction

Cartographic modeling (also known as map algebra) is a powerful set of operations for manipulating raster geographic data. It treats raster layers as variables that can be transformed or combined into new layers by using primitive operations. Cartographic modeling (CM) operations are based on the raster data model because raster data have a simple data structure that is computationally efficient and permits a large variety of data analysis operations. Based on spatial scope, primitive operations are divided into three groups: local, focal, and zonal (Tomlin, 1990). Local functions are cell-by-cell operations that use the input raster layers to compute cell values at the same location for the output raster layer, which means that the value of each new pixel is defined by the values of the same pixel on the input layer(s). Focal operations calculate a focus cell value using the cell values within a neighborhood of the focus cell. Common spatial neighborhoods include rectangles, circles, and wedges. Zonal operations utilize a zone layer and a value raster layer as inputs and calculate a value for each cell using the cell values in the same zone into which the cell falls. Zones are defined by the cells which have the same value on the zone layer.

A raster layer in conventional cartographic modeling represents the spatial distribution of an environmental variable measured at a particular moment or during a certain period of time. Because of the lack of a temporal dimension, only non-temporal spatial analysis can be performed on the raster layer and thus conventional cartographic

modeling does not offer operations to analyze spatiotemporal data. In the real world, however, very few geographic phenomena and processes are static so that the temporal dimension should always be considered in analyses (Dalton, 2005). In addition, developments in data collection techniques, especially remote sensing, have produced a large number of spatiotemporal datasets. For example, Normalized Difference Vegetation Index (NDVI) data have been available bi-weekly since the 1970s; MODIS has been providing global daily snow cover data since 2002; and the NEXRAD system has been providing hourly precipitation data since the early 1990s. These spatiotemporal data offer the opportunity to explore and study spatiotemporal processes that are essential to the understanding of earth systems. Unfortunately, analyzing these data is hindered by the lack of spatiotemporal analysis functions in current GIS (Mannis, 2005).

Although some GIS functions can visualize spatiotemporal datasets (for example, the Tracking Analyst extension in ESRI ArcGIS), few have the ability to analyze spatiotemporal datasets. Taking zonal operations as an example, zones are always defined only in the spatial dimension and the operations are performed within the spatial scopes of the zones. But with spatiotemporal data, where the time scope is added, zones can be defined in either the spatial or temporal dimensions or both, and zonal operations can be extended to be performed in spatiotemporal scopes.

Besides the temporal limitation, conventional CM operations can only be applied on raster layers. This is problematic because some geographic phenomena are better

represented as vector features than raster layers. For uncontinuous geographic features such as roads, streams, and residents houses, these are better represented by vectors than rasters. To overcome this shortage, progress has been made for CM operations on vector data (French and Li, in press), but there is still no corresponding analysis framework available in the vector data model. A further extension to conventional CM would allow spatiotemporal zones defined in the vector data model. In response to the increasing availability of spatiotemporal data and the demand for spatiotemporal analysis, this research extends the zonal operations in conventional cartographic modeling to handle spatiotemporal datasets.

In chapter two, I reviewed the extensions of CM that have been made for implementing spatiotemporal analysis in GIS and illustrated the three basic types of spatiotemporal zones. In chapter three, I explained what the NEXRAD precipitation data is and why the NEXRAD is a good database source for spatiotemporal analysis. In Chapter four, I introduced the components of the Nextool software package and how we can use the tool to implement diverse of applications that are corresponded with NEXRAD precipitation data. A case study was provided to illustrate the ability of using vector spatiotemporal zonal operations to generate certain time precipitation input files for non-point source pollution models. In Chapter 5, I describe how we can use flow length and antecedent time period to define spatiotemporal zones and use them to explore the effects of antecedent precipitation on water quality. In Chapter 6, I made the

conclusions of the thesis and also point out some future researches that I haven't described sufficiently in this article but certainly would like to have for the further study.

Chapter 2. Extending Cartographic Modeling for Spatiotemporal Process

2.1 The Development of Spatiotemporal Data Analysis

In recent years, a growing number of researchers have been using spatiotemporal analysis to understand dynamic geographic phenomena. They have been using time series images or photos to detect climate change (Stern, 2005), monitor ecological systems change (Pettorelli et al., 2005) and urban growth (Tachizuka et al., 2005). For GIS functions part, Yuan (1996 and 2001) described a framework for representing complex geographic phenomena in both the spatial and temporal dimensions and a framework for implementing temporal GIS analysis. In the framework, where and when precipitation events occur and how precipitation processes progress in geographic space and over time are explicitly stored. Nadi and Delavar (2001) argued that a temporal database, visualization, and analysis should be added as essential components in GIS. They developed a prototype temporal GIS to simulate traffic information using a cadastral map. Turner (2007) developed a GIS-based approach to implement spatial and temporal analysis of landscape patterns and found out that spatiotemporal GIS CM functions can play an important role for ecological topics. Many spatiotemporal analysis GIS functions have been developed, but most of them can only visualize dynamic geographic processes such as Yuan's research and provide limited or ad hoc (for specific use but not general) analysis functions and few cartographic modeling operations have been systematically proposed to match the increasing demand for spatiotemporal analysis.

2.2 Cartographic Modeling Operations and Its Extensions

Extensive work has been done to extend the cartographic modeling framework for GIS applications. In addition to early work on the raster data model (Tomlin 1990), cartographic modeling operations were developed for vector data model where cell values are vectors rather than scalar measurements (Li and Hodgson, 2005). Wang and Pullar (2005) also applied cartographic modeling operations to physical processes described by vector fields. Tobler (1995) and Ledoux et al. (2006) extended cartographic modeling operations to irregular polygons where neighborhoods and zones are defined by polygons. All these extensions to CM assume the data layers are snapshots of dynamic geographic processes and did not consider the time scope as a dynamic variable. On the other hand, Yuan (2001) and Mennis and Peuquet (2003) developed some cartographic modeling concepts and functions to identify spatiotemporal zones for specific spatiotemporal raster datasets, but they did implement these for vector datasets. Furthermore, based on the concept of the spatiotemporal 'data cube' (Raper and Livingstone, 1995; Mennis, 2003), Mennis et al. (2005) developed what they called "cube–functions" to handle raster spatiotemporal data cubes consisting of two spatial dimensions and one temporal dimension. Although they proposed cubic local, focal, and zonal operations for spatiotemporal raster data, they did not provide details on how various kinds of spatiotemporal neighborhoods and zones could be defined. In addition, their operations could only be applied to raster data.

2.3 Cartographic Modeling Zonal Operations in the Temporal Dimension

Since zonal operations obviously require zones, defining zones is the initial step for performing a zonal analysis. In conventional cartographic modeling, zones are defined by a set of cells in two-dimensional space. By adding the temporal dimension, zones can be defined by using only spatial scope, using only temporal scope, and using spatiotemporal scope for spatiotemporal analysis. Mennis et al. (2005) proposed cubic map algebra to handle raster spatiotemporal data, which turns two-dimensional cells into three-dimensional cubes by adding the time dimension. With spatiotemporal cubes, locations, zones, and neighborhoods can be defined in cubic form (Figure 2-1). The cubic CM extends raster square cells into cubes. Figure 2-1a illustrates how a local sum function can be performed with two spatiotemporal cubic layers. Here each cube has a values and the result cube will have a new value by adding two cubes together which these two cubes have the same row and column number. Figure 2-1b shows how a 3x3 focal neighborhood (row and column) could be extended into a 3x3x3 spatiotemporal focal neighborhood (row, column, and timesteps). And Figure 2-1c gives an example of a zonal sum operation with a value cube and zone cube. There are three zone cubes for the zone cube, from gray to black. They varies both over space and time. And the value cubes within different cube zone are added to get a new value for the result table.

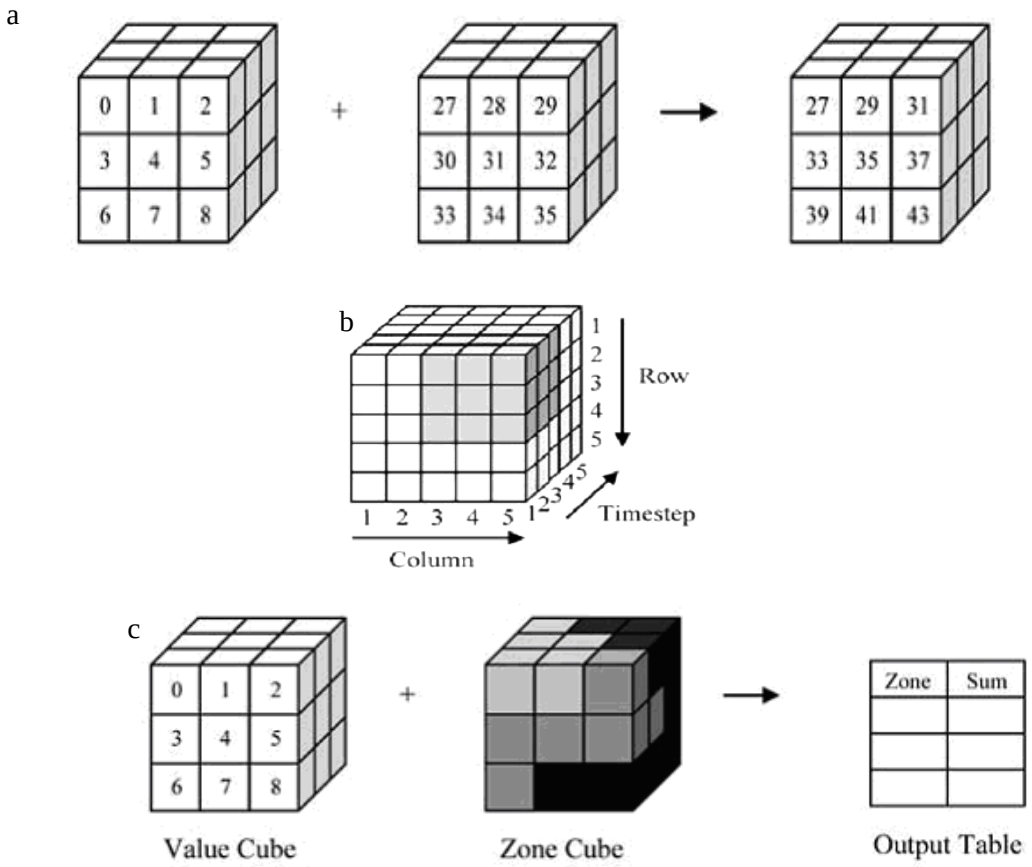

Figure 2-1. Cubic CM operations (Mennis et al, 2005). (a) Three-dimensional CM local function, (b) Three-dimensional CM 3x3x3 focal neighborhood, (c) Three-dimensional CM zonal function.

For cubic zonal operation, three types of zones can be defined for spatiotemporal datasets and analysis (Mennis et al. 2005). The first type of zone varies only over space but not in time (figure 2-2a). The second type of zone varies only over time but not in space (figure 2-2b). And the last type of zone varies both in space and time (figure 2-2c).

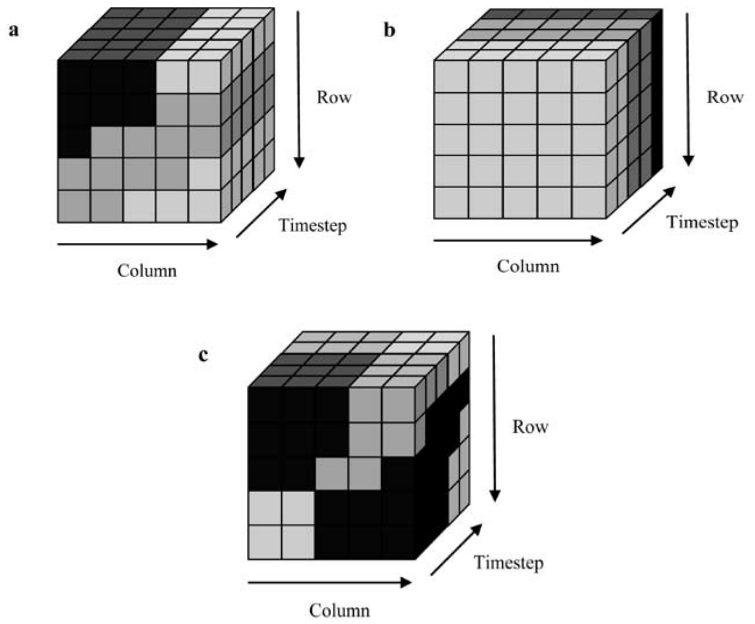

Figure 2-2. Types of zone cubes used in spatiotemporal zonal operations (Mennis et al, 2005). (a) A zone cube that varies only over space but not in time; (b) A zone cube that varies over time but not in space; and (c) A zone cube that varies in space and time.

While Mennis et al. (2005) pioneered cubic map algebra, they did not provide a systematic approach for defining temporal neighborhoods and zones. In addition, their cubic operations only work in the raster data model. In this study, I used sub-watersheds, flow length and antecedent time periods to define vector spatiotemporal zones and perform spatiotemporal vector zonal sum operation with NEXRAD data. Two applications were also provided to demonstrate the use of the spatiotemporal zones to generate watershed daily precipitation for non-point source pollution models and to explore the effects of antecedent precipitation on water quality.

Chapter 3. NEXRAD Spatiotemporal Data

The Next-Generation Radar (NEXRAD) system is a network of over 150 high-resolution Doppler weather radars operated by the National Weather Service (NWS). It detects precipitation and atmospheric movement (or wind) and returns data that can be displayed in a map showing patterns of precipitation or wind and their changes over time. For years, NEXRAD radar-based estimates were combined with rainfall data from real time rain gauge stations to make multisensor precipitation estimates (MPE) (Krajewski 1987). NWS River Forecast Centers (RFCs) produce regional multisensor precipitation products using information from numerous WSR-88D radars and a network of gauges that send data to RFCs in near real-time (Fulton, 1998). These NEXRAD multisensor precipitation estimates are widely used to detect severe wind, hail, and tornadoes and for improved hydrological forecast operations and services (Fulton, 2002). In addition, NEXRAD precipitation products have also been used to analyze the statistical characterization of extreme rainfall frequency and to validate satellite remote sensing algorithms (Krajewski and Smith, 2002; Habib and Krajewksi, 2003). A long period of NEXRAD precipitation data is a critical input for hydrological modeling, weather and climate modeling, and drought monitoring and it is an excellent dataset for spatiotemporal analysis using due to its good temporal resolution (every hour)..

NEXRAD produces precipitation estimates at a higher temporal (one hour) and spatial (4 km x 4 km) resolution than has traditionally been available for hydrological

modeling, and several levels of NEXRAD data products are available. The lowest level NEXRAD data product (Stage I) only uses radar information to estimate hourly rainfall. Stage II NEXRAD data product are improved by combining rain gauge data, satellite information, and surface temperature information from Stage I data. In Stage III, after being calibrated with gauge observations and combining individual radar observations, data from several radars are used to generate the rainfall estimates in a common grid system so that the NWS RFCs can use these estimates to forecast basin-wide stream flow (NOAA and NWS websites). As a higher level of NEXRAD data product, multiple weather radars covering an entire river basin are combined using the average of available estimates for each grid cell (Fulton et al., 1998).

The multisensor precipitation estimator (MPE) data uses rain gauges and the GOES satellite to reduce existing biases in radar rainfall estimates and produces a radar-gauge-satellite precipitation product. The MPE precipitation data was introduced in 2002 and has been replacing the Stage III precipitation data since 2003. The Stage III and MPE datasets are especially valuable for hydro-meteorological applications since rainfall is corrected using multiple surface rain gauges and their quality is controlled through interactive quality control by the Hydrometeorological Analysis and Service (HAS) forecasters at individual River Forecast Centers (RFCs) (Fulton et al., 1998; Young et al., 2000). All of these data are in the Hydrological Rainfall Analysis Projection (HRAP)

coordinate system. HRAP cell size is 4.00 km and is defined in a polar stereographic map projection using a spherical earth datum (Reed and Maidment, 1999).

Both the Stage III and MPE precipitation data are broken down into 13 separate geographical regions (Figure 3-1). Each region covers a NWS-designated river basin. The temporal coverage of the dataset in each river basin varies. For instance, Stage III data in the Arkansas Red River Basin (ABRFC) extend back to May 1993, while the latest RFC region, San Juan only extends back to March of 2000. Both datasets can be downloaded from the NOAA website http://dipper.nws.noaa.gov/hdsb/data/nexrad/nexrad.html or from individual RFCs.

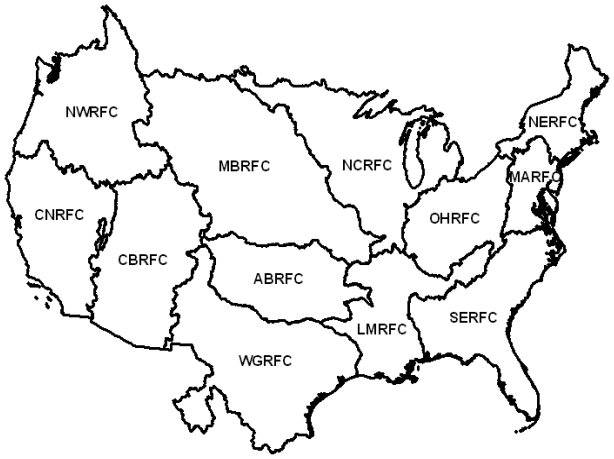

Figure 3-1. Twelve NWS river forecast centers in which Stage III and MPE NEXRAD precipitation data are distributed. Note that the Alaska River Forecast Center (AKRFC) is not shown in the figure.

Chapter 4. Generating Precipitation Inputs for Non-point Source Pollution Models

4.1 Overview

Precipitation data are critical to non-point source pollution modeling (NPSPM) applications. Traditionally, precipitation is only measured at weather stations scattered in space. Spatial and temporal distribution of precipitation is typically obtained through various interpolation methods. Those methods, however, may not be able to characterize the significant spatial and temporal variations in precipitation. NEXRAD has the capability of capturing both the spatial variation and dynamic nature of rainfall and, therefore, has the potential to provide better spatiotemporal precipitation data as the technology advances (Garbrecht et al., 2001; Ogden et al., 2001). Unfortunately, NEXRAD precipitation data is difficult to use due to its unfamiliar file formats and coordinate system, large dataset size, and the lack of spatiotemporal analysis tools. The combination of these factors hinders both researchers and practitioners from using the NEXRAD precipitation datasets for NPSPM applications. Recognizing these problems, I developed a software toolset which can manage, visualize, and calculate daily precipitation for non-point source pollution models, such as AnnAGNPS and SWAT (see appendix for more details about these two models).

I chose MATLAB© to develop the toolset. MATLAB has a file format (.mat) which has very good data compression capability. With 11 years of hourly NEXRAD precipitation data, the average hourly file size stored in MATLAB format, NEXRAD raw binary

format, and ESRI ASCII GRID© format are 7.8 KB, 105.4 KB, and 468.9 KB, respectively. Second, MATLAB offers a scripting environment that can handle large spatiotemporal datasets reliably and has many built-in functions for manipulating multidimensional datasets. A few GIS functions such as projection, extraction, and intersection are also available through the Mapping Toolbox in MATLAB. Third, it is easy to develop graphical user interfaces (GUI) and to compile MATLAB scripts into standalone Windows applications. Fourth? Deployment of a Windows application does not require a MATLAB license. The toolset is available either as MATLAB scripts (i.e., m-files) or a standalone Windows application.

4.2 Building NEXRAD Precipitation Databases

The first step in using NEXRAD data for spatiotemporal analysis is to create a precipitation database. In the current NEXRAD data distribution from the NOAA web site, both Stage III and MPE hourly binary files are compressed in .gz format. All the compressed hourly files for a single day are then tarred into a daily file, which in turn is compressed into a monthly file. This compression structure is used to save total storage space and increase distribution throughput on the Internet. Both Stage III and MPE NEXRAD unzipped hourly files are stored in a binary format called XMRG. The database tools in the MATLAB toolset can be used to create a new database, open, or get the metadata of an existing NEXRAD precipitation database from the above data format. In the current implementation, a database is a folder under which hourly precipitation

files are stored. These hourly binary files are then converted from the XMRG format to MATLAB format by a compiled C program within MATLAB (i.e., the MEX function). This compiled C program is a modified version based on the C program provided by the NWS at http://www.nws.noaa.gov/oh/hrl/dmip/nexrad.html. Each hourly file in the database has a unique name indicating a time stamp, which is obtained from its original XMRG file name. In addition to this above, the NexTool database creation function also creates a file (i.e., DBInfo.mat), which stores important metadata for the precipitation database. Information in the file includes the precipitation unit, spatial and temporal extents, and spatial and temporal reference systems. The tool can process Stage III and MPE data spanning from a few hours to several years. Depending on NEXRAD data size and duration, this tool can run from a few seconds to hours to create a precipitation database.

4.3 Coordinate System Conversion

Both Stage III and MPE precipitation data are mapped in the Hydrologic Rainfall Analysis Projection (HRAP) coordinate system (Greene and Hudlow, 1982). The HRAP coordinate system is based on a conformal polar stereographic map projection, which uses a projection plane that is parallel to the equatorial plane and intersects with a reference spheroid at the latitude of 60º. The origin of the map projection is located at the intersection of latitude 60º N and longitude 105º W. The equations to perform forward and backward transformation between HRAP geographic coordinates (i.e., latitudes and

longitudes) and HRAP projected coordinates are provided by Reed and Maidment (1999). The toolset provides two tools to project and unproject between geographic coordinates defined on NAD83 and the HRAP coordinate system. And supports both vector and raster data. The toolset accepts vector datasets in the Shapefile© format and raster datasets in the ESRI ASCII GRID format.

4.4 Data Exporting and Visualization

Hourly precipitation in the NEXRAD database can be extracted at points or within rectangular regions and aggregated into daily precipitation. Extracted daily precipitation is exported as text files that can be examined by text editors or imported into GIS as raster layers. ,The toolset provides a tool that generates a polygon shapefile representing NEXRAD cells and/or a point shapfile representing the centers of the NEXRAD cells. These shapefiles are created in HRAP coordinates but they can be converted into NAD83 geographic coordinates by using the coordinate conversion tools, which enable them to be well used in various GIS environments. A very preliminary visualization tool is also provided to show hourly precipitation within a certain period of time within a RFC. The animation can be directly seen within the toolset's display window or saved as a movie file, which can then be viewed using compatible movie players.

4.5 Generating Precipitation Input Files for AnnAGNPS and SWAT

While NEXRAD precipitation is estimated at square cells, the precipitation inputs for most non-point source pollution models, such as AnnAGNPS and SWAT, are

typically based on irregular sub-watershed polygons at a daily scale. Essentially, an aggregation operation within a spatiotemporal zone is needed. This aggregation operation is a spatiotemporal zonal sum operation where the spatial dimensions of the spatiotemporal zones are defined by the sub-watersheds and the temporal dimensions are 24 hours (one day). These spatiotemporal zones, which vary over both in space and time, belong to the third type of spatiotemporal zone discussed in section 2.3 (figure 2-2c). Figure 4-1 illustrates how the spatiotemporal vector zone is defined for one watershed and three days.

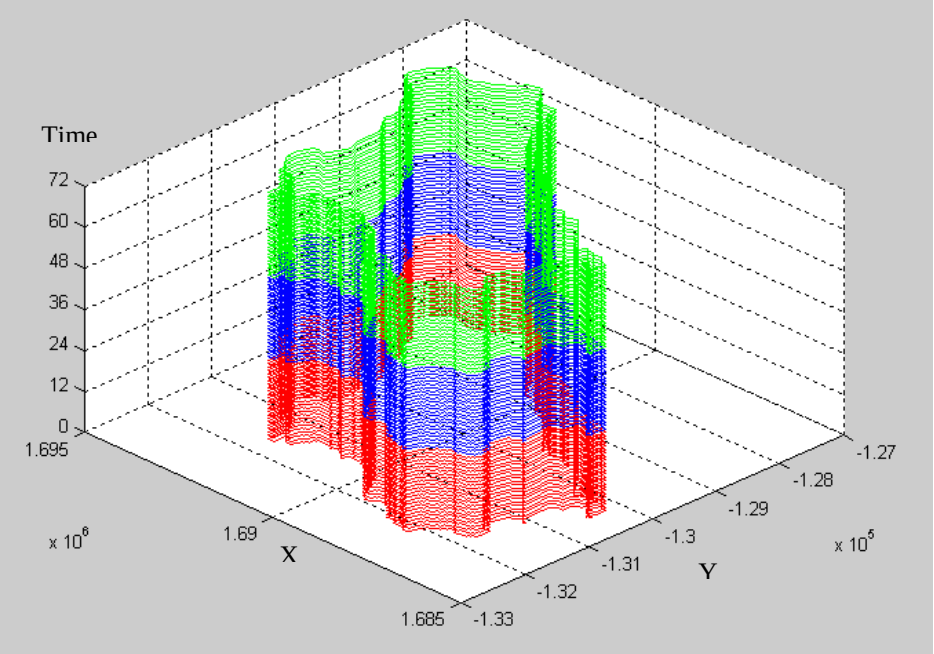

Figure 4-1. Vector spatiotemporal zones used to calculate daily precipitation inputs for non-point source pollution models. The red zone is the first 24 hours for a sub-watershed. The blue zone is the second 24 hours and the green is the third 24 hours.

Hourly NEXRAD precipitation can be aggregated into the sub-watershed zone using different approaches. For AnnAGNPS, each sub-watershed is assigned to the precipitation of the NEXRAD cell which covers the largest portion of the sub-watershed. For example, precipitation in the sub-watershed (i.e., a zone) indicated by a dashed line in in Figure 4-2a would have the value of P_5 since this NEXRAD cell covers the largest portion of the sub-watershed . This approach of estimating sub-watershed precipitation is appropriate when the sub-watersheds are smaller than NEXRAD cells, which is the case in AnnAGNPS models.

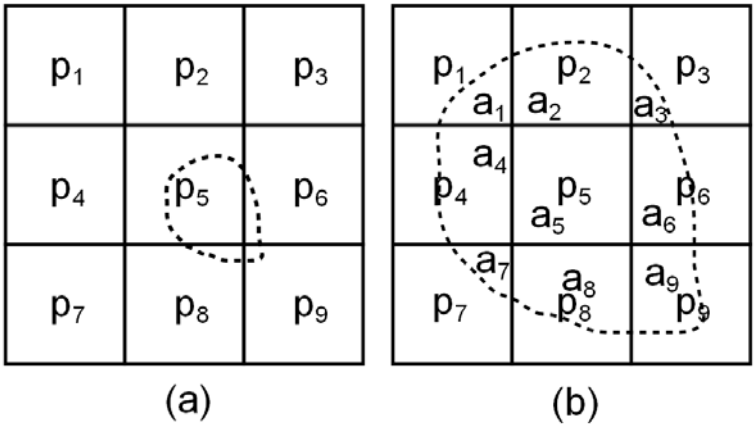

Figure 4-2. Two methods of deriving sub-watershed precipitation from NEXRAD cell precipitation. (a) Each sub-watershed is assigned the precipitation of the NEXRAD cell which covers the largest area of the sub-watershed. (b) Sub-watershed precipitation is calculated based on an areal interpolation.

For SWAT, sub-watershed precipitation is calculated based on the concept of areal interpolation. For the example in figure 4-2b, the precipitation of the sub-watershed indicated by a dashed line is calculated using the following equation:

$$p = \frac{\sum_{i=1}^{9} p_i * a_i}{\sum_{i=1}^{9} a_i} \quad (1)$$

where p_i is the precipitation at nine NEXRAD cells and a_i is the intersection area between each NEXRAD cell and the sub-watershed. This approach is more accurate than the one above and should be used when sub-watersheds are larger than NEXRAD cells. After hourly precipitation is calculated within sub-watersheds, each hourly precipitation can then be added together to get daily precipitation files for use as precipitation inputs in the models.

Chapter 5. Exploring the Effects of Antecedent Precipitation on Water Quality

5.1 Overview

Many studies have used watersheds as spatial zones to monitor ecologic changes. Martinko et al. (2007) proposed an ecoregional classification system to assess biological impairment of watersheds. They used vegetation phenology metrics (VPMs), which were derived from 10 years of Advanced Very High Resolution Radiometer (AVHRR) satellite time-series images, as dynamic landscape indicators to estimate water quality inside watersheds. Their primary research goal was to predict watershed water quality through VPMs. Although there generally was a good relationship between VPMs and water quality, Martinko et al. found some water sample outliers that did not fit the relationship. One possible factor that may have caused such outliers is the antecedent rainfall within the watersheds of the water samples. Several studies (Jackson et al, 1993; Salamanca et al, 2002) have shown that rainfall is a very important short-term factor affecting the environment, especially in semiarid and arid areas.

In this chapter, I used a vector zonal operation and the NEXRAD precipitation database to explore the effects of antecedent precipitation on water quality. Here antecedent precipitation is the cumulative rainfall occurring hours or days before water samples were collected. For a specific water sample, the watershed of the water sample and flow length of the watershed were used to define the spatial extent of a spatiotemporal zone and a certain number of hours before the water sample was taken

was used to define the temporal dimension of the spatiotemporal zone. Accumulated precipitation from those spatiotemporal zones was extracted and the relationship between water quality and antecedent precipitation was explored.

5.2 Study Area

The study area is located in the Arkansas Red River Basin (Figure 5-1). A total of 1,406 water samples were collected by the Kansas Biological Survey (KBS) from 1992 to 1999. Ninety percent of the water samples were located in the eastern part of the basin. Table 5-1 shows a small portion of the samples. There are several attributes within the table. The “Name” field is the location where the water samples were taken. The “Date” field is the date when the water samples were collected. The fields “Total P (mg/l)”, “Turbidity (NTU)”, and “Total N (mg/l)” store water quality measurements. From the table we can see that some water samples were collected at the same location but at different times. As a result, there are only 89 unique spatial locations among the 1,406 samples. Each location was sampled about 16 times on average.

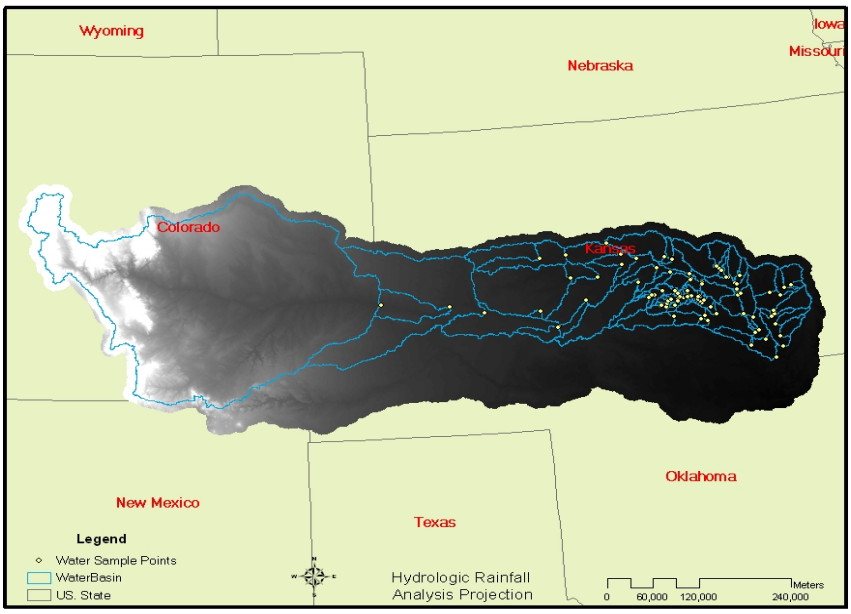

Figure 5-1. Water samples within the Arkansas Red River Basin. Yellow dots are water sample locations. Polygons with blue outlines are sub-watershed associated with each water sample points. Raster layer is the DEM data for ABRFC. And the background is the boundary map of U.S. State.

Table 5-1. Fifteen water quality sample data collected by Kansas Biological Survey (KBS). There are a total of 1,406 water samples.

Name	Date	Total P (mg/l)	Turbidity (NTU)	Total N (mg/l)
LITTLE COW CREEK NEAR LYONS	17-May-1999	1.289999962	405	
ARKANSAS RIVER NEAR FORD	7-Jun-1999	0.600000024	350	
COWSKIN CREEK NEAR BELLE PLAINE	9-Jul-1999	0.539065003	330	1.77
ARKANSAS RIVER NEAR KINSLEY	8-Jun-1999	0.579999983	325	
ARKANSAS RIVER NEAR DEERFIELD	7-Jun-1999	0.419999987	315	
ARKANSAS R. NEAR ARKANSAS CITY.	18-May-1999	0.959999979	295	
ARKANSAS RIVER NEAR KINSLEY	10-Aug-1999	0.670000017	295	
BLACK KETTLE CREEK NEAR HALSTEAD	15-Sep-1999	0.689999998	295	
ARKANSAS RIVER AT OXFORD	18-May-1999	0.860000014	290	
ARKANSAS RIVER NEAR DUNDEE	8-Jun-1999	0.519999981	280	
COWSKIN CREEK IN WICHITA-VALLEY CENTER FLOOD	17-May-1999	0.930000007	265	
ARKANSAS RIVER NEAR FORD	9-Aug-1999	0.850000024	245	
WALNUT RIVER AT GORDON	18-May-1999	0.649999976	245	
ARKANSAS R. NR GREAT BEND, KS.	9-Jun-1999	0.50999999	240	
ARKANSAS RIVER NEAR DUNDEE	10-Aug-1999	0.870000005	240	

5.3 Water Quality and Antecedent Precipitation

5.3.1 Method

The approach for this analysis was to calculate the amount of antecedent precipitation within the spatiotemporal zone associated with each water sample and to examine the relationship between water quality and antecedent precipitation, i.e., whether antecedent precipitation (the independent variable) is correlated with water quality measurements (dependent variables). After consulting with water quality experts at KBS, two water quality measurements, total amount of phosphorus (Total_P) and water turbidity, were used to explore the effects of antecedent precipitation on water quality. Various researchers have also demonstrated that high values of these two variables usually indicate poor quality of stream water (Martinko et al., 2007; U.S. EPA, 1989; Buttner et al., 1993).

Because the sub-watersheds associated water quality samples vary over space and the sampling dates are different, the spatiotemporal zones used for this approach are the same as the previous spatiotemporal zones (Figure 4-1), which were used to calculate sub-watershed daily precipitation for non-point source pollution models. As a result, this type of spatiotemporal zones would vary over both space and time. Table 5-2 provides two examples of water samples which were taken at different places and times. Figure 5-2 shows how two spatiotemporal zones were defined for the water samples with an antecedent time of 5 hours. The total amount of precipitation within the spatiotemporal zones is calculated using the areal weighted zonal sum operation discussed in section 4.6.

Table 5-2. Water sample points table (two samples)

IDCPCB	Date	Total P (mg/l)
1272a	10/10/1999	0.167
1224b	10/9/1999	0.458

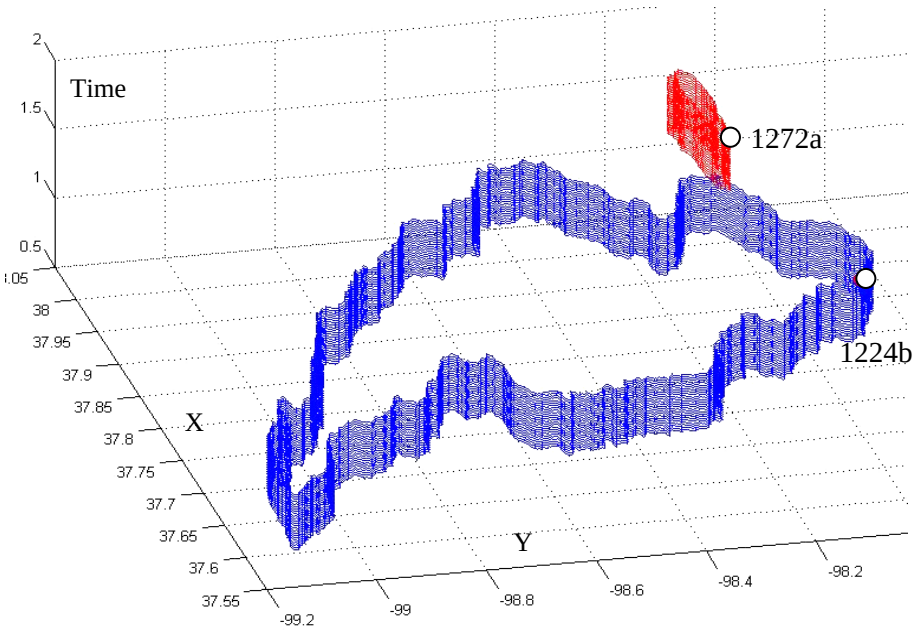

Figure 5-2. Spatiotemporal zones associated with two water samples in Table 5-2. Red circles are water sample points in space and time. Blue and red walls represent the spatiotemporal zones associated with the water samples.

There were 1,406 water samples taken at 89 different locations from 1992 to 1999. However, because the NEXRAD precipitation data only cover the time period from 1995/10/01 to 2007/12/31, there are only 799 samples at 87 unique spatial locations that could be used for this analysis. Instead of just using entire watersheds as the spatial zones, I created several spatiotemporal zones for each watershed. Those spatiotemporal zones are defined by different flow lengths within the watersheds and antecedent time periods. This approach would allow us to identify the flow length which is critical to water quality. Several antecedent time periods from 0 to 4 hours to 0 to 36 hours before water samples were taken were also used for the same purpose of identifying critical time periods that might be important to water quality.

the flow lengths of the 87 watersheds varied considerably. Figure 5-3 shows the distribution of the maximum flow lengths in the 87 watersheds. The shortest flow length is about 4 km and the longest one is about 1230 km. Flow length increases slowly until the 77th watershed. There is a obveious change from the 77th watershed to the 78th watershed, where flow length jumps from aound 320 km to 630 km. The following nine flow lengths increase

nearly linearly from 630km to 1230km. With the help from Dr. Li, I developed fourteen critical flow length values to make sure various flow lengths are sampled for the watersheds. The first threshold value is 4.14 km, which allows all the watersheds to be used in the statistical analysis. The second threshold is the average value of the first 10 flow lengths, which is 9.87 km. The third one is the average value from the 11th flow length to the 20th flow length, which is 21.67km. By repeating this step, I got the first 8 flow length threshold values, which ended at the 70th flow length. Because there is a significant change from the 77th flow length to the 78th, a different method was applied. From the 71st flow length to the 74th flow length, I calculated the average value as the 9th threshold value. From the 75th to the one which has a flow length value of 320 km, I calculated the average value as the 10th threshold value. Between 320 km and 630 km, two values (430 km and 530 km) were chosen as threshold values. The last threshold value, 972.24 km, was calculated by averaging flow length from 630 km to the last flow length value. After these steps, 14 flow length threshold values were used to define flow length zones. These critical values were subject to my personal study to reduce the flow length change issue. Table 5-3 shows the flow length threshold values and the number of watersheds included with those threshold values.

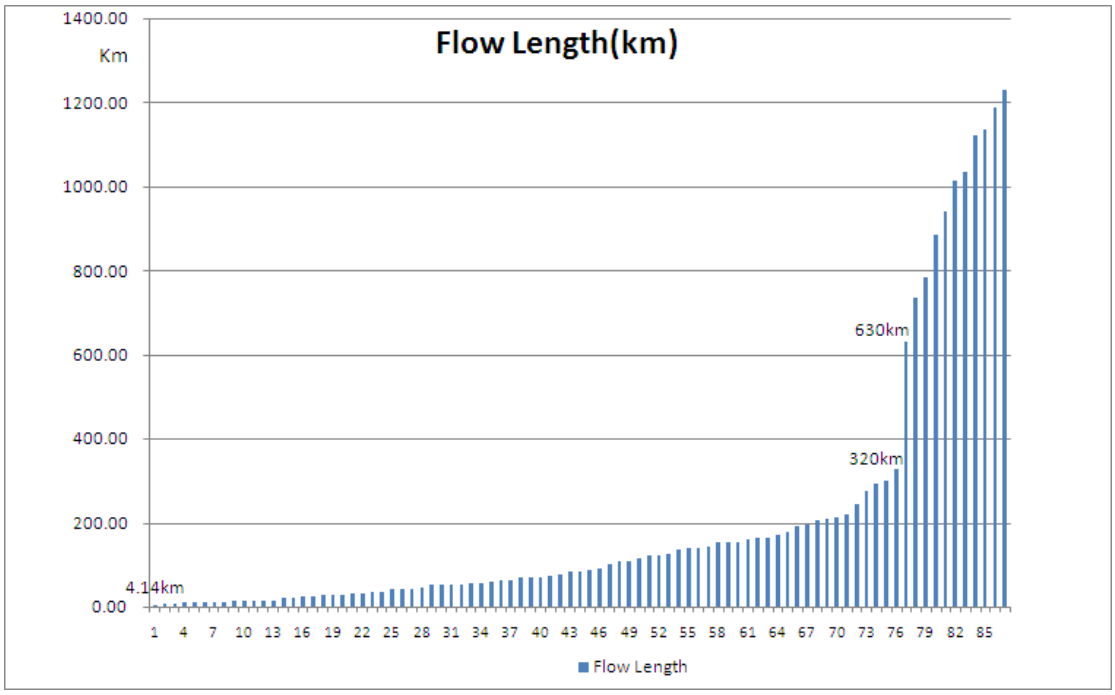

Figure 5-3. Maximum flow lengths of the 87 watersheds.

Table 5-3. Flow length threshold values and the number of watersheds included.

Flow length	Number of watersheds included
0 – 4.14km	87
0 – 9.87km	85
0 – 21.67km	73
0 – 40.49km	64
0 – 61.36km	53
0 – 92.43km	42
0 – 138.79km	34
0 – 184.74km	23
0 – 257.89km	16
0 – 328.02km	12
0 – 430km	12
0 – 530km	12
0 – 630.95km	11
0 – 972.24km	7

Besides using different flow lengths as spatial zones, several temporal zones were also used in this analysis. After discussions with water quality experts at KBS, I recognized that 36 hours would be the longest time that antecedent rainfall might affect water sample quality and 4 hours would be an appropriate interval to divide 36 hours into nini temporal zones.

Each combination of a flow length zone and an antecedent time zone defines a spatiotemporal zone for a water sample. This means that each water sample would have at least nine antecedent precipitation values (when the watershed only has one flow length zone) to at most 126 antecedent precipitation values (when the watershed has 14 flow length zones). The antecedent precipitation values within these spatiotemporal zones were first calculated. A correlation coefficient matrix was then generated by calculating correlation coefficients

between antecedent precipitation and water quality measurements for each spatiotemporal zone. Relatively higher correlation coefficients in the matrix would indicate the spatiotemporal zones within which antecedent precipitation give more affects to water quality.

5.3.2 Statistical Results for Total Amount of Phosphorous

Using these spatiotemporal zones, antecedent precipitation values for each water sample in space and time were extracted. Because the antecedent precipitation values could be zero, statistic analysis was performed in two ways, one included zero antecedent precipitation and the other only used non-zero antecedent precipitation. Table 5 – 4 contains the correlation coefficients between all antecedent precipitation (including zero precipitation) and total amount of phosphorous between the water samples.

Table 5-4. Correlation coefficients between antecedent precipitation and total amount of phosphorous for each spatiotemporal zone. Numbers in parentheses in the first column are the number of water samples. Numbers in the parenthesis in the rest of the columns are the P-values of the correlation coefficients.

Time / FL(km)	0-4 hours	0-8 hours	0-12 hours	0-16 hours	0- 20 hours	0-24 hours	0-28 hours	0-32 hours	0-36 hours
0 – 4.138 (804)	0.045 (0.1987)	0.0573 (0.1046)	0.0782 (0.0267)	0.1148 (0.0001)	0.1293 (0.0002)	0.1289 (0.0003)	0.1278 (0.0003)	0.1374 (9.42E-05)	0.148 (2.54E-05)
0 – 9.867 (804)	0.0351 (0.3205)	0.0543 (0.1241)	0.0778 (0.0275)	0.1138 (0.0012)	0.1235 (0.0005)	0.1217 (0.0005)	0.1230 (0.0005)	0.1306 (0.0002)	0.1391 (7.63E-05)
0 – 21.666 (795)	0.0523 (0.1405)	0.0564 (0.1118)	0.0759 (0.0324)	0.109 (0.0021)	0.1111 (0.0017)	0.1086 (0.0002)	0.1095 (0.0002)	0.1166 (0.0009)	0.1241 (0.0005)
0 – 40.497 (747)	0.0481 (0.1889)	0.0453 (0.2159)	0.0651 (0.0755)	0.0918 (0.0121)	0.1088 (0.0029)	0.1045 (0.0043)	0.1056 (0.0039)	0.1163 (0.0015)	0.1214 (0.00083)
0 – 61.364 (699)	0.0246 (0.5163)	0.0423 (0.2645)	0.044 (0.2450)	0.0291 (0.4423)	0.0294 (0.4372)	0.0348 (0.3582)	0.0365 (0.3348)	0.0385 (0.3093)	0.0434 (0.2513)
0 – 92.429 (605)	0.008 (0.8438)	0.0013 (0.9738)	0.044 (0.9139)	0.047 (0.9769)	0.0038 (0.9245)	0.0024 (0.9519)	0.0027 (0.9471)	0.0022 (0.9558)	0.0122 (0.7627)
0 – 138.794	0.0659	0.0435	0.0362	0.0109	0.048	0.0015 (0.9707)	0.003 (0.9429)	0.0033 (0.9366)	0.0063 (0.881)

(562)	(0.1182)	(0.3027)	(0.3915)	(0.7964)	(0.9087)				
0 – 184.739 (468)	0.0541 (0.2336)	0.0398 (0.3813)	0.0319 (0.482)	0.05 (0.2703)	0.0416 (0.36)	0.0404 (0.3736)	0.0434 (0.3393)	0.031 (0.494)	0.0396 (0.3827)
0 – 257.894 (376)	0.0491 (0.3422)	0.0155 (0.7635)	0.0141 (0.7848)	0.0359 (0.4869)	0.0332 (0.52)	0.0427 (0.4083)	0.0414 (0.4224)	0.0459 (0.374)	0.0521 (0.3127)
0 – 328.024 (296)	0.0498 (0.393)	0.0414 (0.477)	0.0378 (0.5163)	0.004 (0.9448)	0.0298 (0.6089)	0.0174 (0.7653)	0.0107 (0.8539)	0.0029 (0.9597)	0.0017 (0.9759)
0 – 430.00 (240)	0.0549 (0.3966)	0.0462 (0.4755)	0.0448 (0.4894)	0.0417 (0.5201)	0.0377 (0.5601)	0.0278 (0.6682)	0.0236 (0.7149)	0.0164 (0.7995)	0.0078 (0.9042)
0 – 530.00 (240)	0.0767 (0.2362)	0.0464 (0.4739)	0.0406 (0.531)	0.0445 (0.4922)	0.0165 (0.799)	0.0121 (0.8508)	0.0131 (0.839)	0.0166 (0.7975)	0.0176 (0.7855)
0 – 630.955 (240)	0.0948 (0.1427)	0.0702 (0.2784)	0.0193 (0.7655)	0.0324 (0.6165)	0.0393 (0.544)	0.0546 (0.3989)	0.0535 (0.4088)	0.0565 (0.3828)	0.0571 (0.378)
0 – 972.235 (227)	0.0892 (0.1803)	0.0669 (0.3148)	0.04955 (0.4574)	0.055 (0.4089)	0.0618 (0.3538)	0.0769 (0.2481)	0.074 (0.2663)	0.0808 (0.2252)	0.0787 (0.2372)

We can see from this table that the correlation coefficients are very low (around 0.1) and they don't indicate a good relationship between antecedent precipitation and total amount of phosphorous. About 80% of the P-values are higher than 0.05, and only the P-values within the first 4 flow lengths and between 12 – 36 antecedent hours are lower than 0.05, indicating these correlation coefficients are statistically significant. The highest correlation coefficient (0.148) comes from the flow length between of 0 and 4.138 km and antecedent time between 0 and 36 hours, which indicates rainfall within that flow length range and that antecedent period affects water quality the most.

Two maps (Figure 5-4a and 5-4b) were created based on the numbers in Table 5-4. Figure 5-4a displays the P-values which are less than or equal to 0.05 (green cells) and the P-values which are greater than 0.05 (purple cells). Figure 5-4b shows the variation of correlation coefficients in the spatiotemporal zones. We can see from these maps that higher correlation coefficients are in the upper right corner within the first 4 rows and they are also statistically significant. In addition, the correlation coefficient values within these spatiotemporal zones (upper right corner) are about 10 times higher than those in other spatiotemporal zones, indicating a possible relationship between antecedent precipitations and total amount of phosphorous within these spatiotemporal zones.

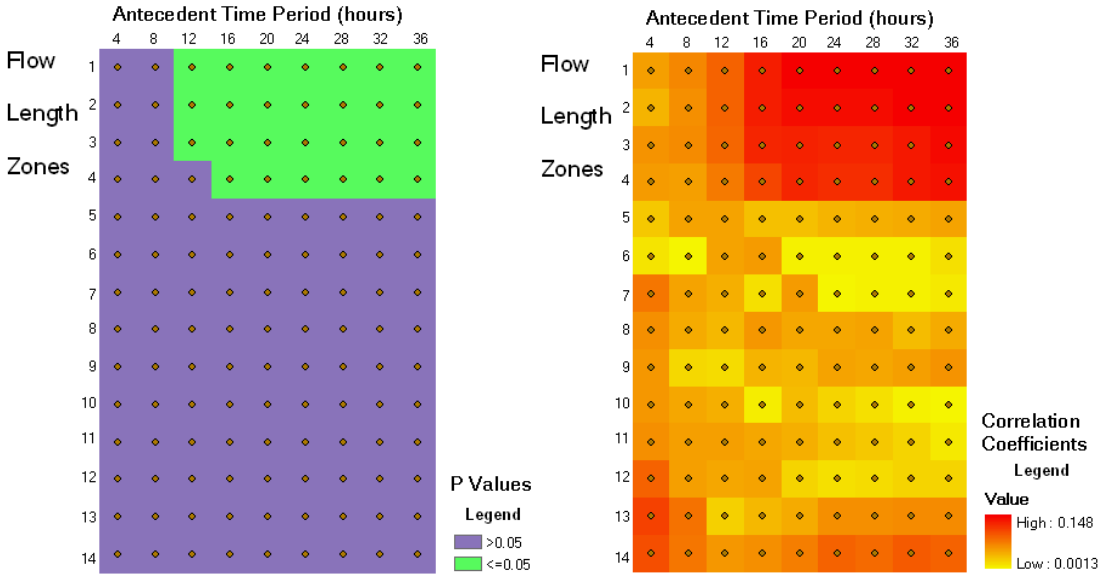

Figure 5-4a & 5-4b. Maps of P-values and correlation coefficients between antecedent precipitations (including zero antecedent precipitations) and total amount of phosphorous for

different spatiotemporal zones. The x-axis is antecedent periods (from 4 hours to 36 hours) and y-axis is flow length zones.

Figure 5-5 shows the significant correlation coefficients of the first 4 flow length zones. From this figure we can see that for the same antecedent time period, the correlation coefficient decreases as flow length increases, and for the same flow length zone, the correlation coefficient increases as antecedent time period increases. This indicates that antecedent precipitation which is closer to the water sample locations would affect water quality more than more distant precipitation, and the longer the antecedent time period is, the more the precipitation affects the total amount of phosphorous.

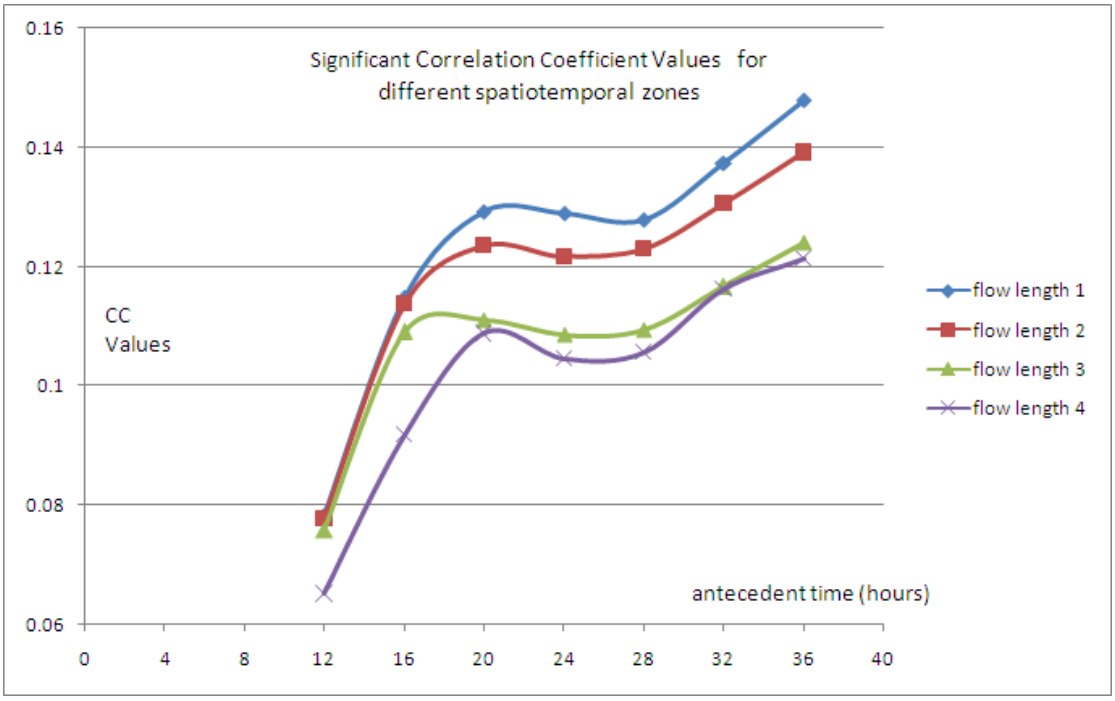

Figure 5-5. Significant correlation coefficients within the first 4 flow length zones.

The correlation coefficients between non-zero antecedent precipitation and total amount of phosphorous were calculated in Table 5-5. The correlation coefficients are higher than those in Table 5-4. However, the coefficients are still low and 78% of the p-values are higher than 0.05, indicating a general non-significant relationship between antecedent precipitation and total amount of phosphorous within most of the spatiotemporal zones.

Table 5-5. Correlation coefficients between non-zero antecedent precipitation and total amount of phosphorous for each spatiotemporal zone. The first numbers in parentheses are the number of water samples and the second number in the parentheses is the p-value of the correlation coefficient.

Time / FL(km)	0-4 hours	0-8 hours	0-12 hours	0-16 hours	0- 20 hours	0-24 hours	0-28 hours	0-32 hours	0-36 hours
0 – 4.138	0.2024 (106, 0.037)	0.0983 (143, 0.242)	0.1591 (176, 0.035)	0.2818 (185, 0.0001)	0.3282 (201, 1.98E-06)	0.2378 (257, 0.0001)	0.3196 (266, 9.86E-08)	0.2786 (301, 9.05E-07)	0.2751 (327, 4.33E-07)
0 – 9.867	0.1053 (94, 0.312)	0.1656 (122, 0.068)	0.3282 (154, 2.4E-05)	0.2839 (164, 0.0002)	0.3026 (178, 4.04E-05)	0.2785 (225, 2.5E-05)	0.2863 (236, 7.84E-06)	0.2395 (280, 5.17E-05)	0.2268 (306, 6.23E-05)
0 – 21.666	0.1827 (103, 0.065)	0.1712 (129, 0.052)	0.1623 (156, 0.043)	0.271 (164, 0.0004)	0.2858 (178, 0.0001)	0.2589 (220, 0.0001)	0.2634 (229, 5.44E-05)	0.2173 (271, 0.0003)	0.2066 (297,0.0003)
0 – 40.497	0.1997 (96, 0.0511)	0.1264 (128, 0.155)	0.1179 (153. 0.1466)	0.2302 (162, 0.0032)	0.2891 (176, 9.95E-05)	0.2646 (224, 6.1E-05)	0.2763 (231, 2.05E-05)	0.2346 (267, 0.0001)	0.1973 (290, 0.0007)
0 – 61.364	0.0881 (91, 0.4064)	0.1209 (129, 0.172)	0.1249 (153, 0.1241)	0.0686 (165, 0.3812)	0.0567 (178, 0.4521)	0.0335 (226, 0.6166)	0.0387 (233, 0.5562)	0.0388 (263, 0.5306)	0.0342 (282, 0.5678)
0 – 92.429	0.0458 (80, 0.6868)	0.0763 (115, 0.418)	0.0749 (141, 0.3776)	0.065 (150, 0.4289)	0.0655 (164, 0.405)	0.03491 (212, 0.6132)	0.03265 (218, 0.6315)	0.0298 (239, 0.6465)	0.03575 (258, 0.5675)
0 – 138.794	0.0277 (71, 0.8183)	0.0391 (109, 0.686)	0.0306 (132, 0.7278)	0.0637 (144, 0.4478)	0.0636 (161, 0.4227)	0.0465 (206, 0.5064)	0.0442 (217, 0.5169)	0.0463 (236, 0.4789)	0.0374 (252, 0.5545)

0 – 184.739	0.2251 (62, 0.0784)	0.186 (93, 0.0742)	0.0778 (107, 0.7997)	0.104 (122, 0.2542)	0.0914 (142, 0.2794)	0.083 (181, 0.2661)	0.0719 (190, 0.3241)	0.0651 (199, 0.3604)	0.0752 (215, 0.2718)
0 – 257.894	0.0957 (56, 0.4827)	0.0428 (81, 0.704)	0.0491 (90, 0.646)	0.0232 (102, 0.8169)	0.0557 (117, 0.5509)	0.0568 (151, 0.4878)	0.0563 (157, 0.4834)	0.0678 (166, 0.3853)	0.0741 (172, 0.3334)
0 – 328.024	0.0953 (45, 0.5333)	0.0413 (61, 0.7522)	0.0078 (68, 0.9491)	0.0114 (85, 0.9178)	0.0782 (94, 0.4537)	0.0612 (122, 0.5029)	0.0315 (129, 0.7226)	0.0303 (137, 0.7248)	0.0258 (141, 0.7613)
0 – 430.00	0.1074 (57, 0.4627)	0.0775 (63, 0.5459)	0.0728 (72,0.5431)	0.0504 (89, 0.6387)	0.0851 (95, 0.4122)	0.0983 (117, 0.2912)	0.0694 (125, 0.4414)	0.0644 (129, 0.468)	0.0571 (133, 0.5134)
0 – 530.00	0.1069 (57, 0.4284)	0.0421 (74, 0.7213)	0.0322 (85, 0.7696)	0.0441 (104, 0.6565)	0.0083 (111, 0.9308)	0.0335 (129, 0.7055)	0.0369 (135, 0.6707)	0.0189 (137, 0.8258)	0.0232 (143, 0.7803)
0 – 630.955	0.1301 (57, 0.3345)	0.0645 (73, 0.5874)	0.0556 (80, 0.6238)	0.0127 (102, 0.8993)	0.0208 (109, 0.8306)	0.0393 (127, 0.6613)	0.0392 (130, 0.6574)	0.0472 (134, 0.5875)	0.0443 (140, 0.6024)
0 – 972.235	0.1087 (76, 0.3501)	0.0558 (84, 0.6137)	0.0242 (96, 0.8144)	0.0289 (115, 0.7587)	0.0492 (120, 0.5931)	0.0505 (149, 0.5404)	0.0514 (152, 0.5293)	0.0698 (153, 0.3911)	0.0676 (153, 0.4061)

Figure 5-6a and 5-6b display the P-values and correlation coefficients shown in table 5-5 as maps. Figure 5-6a displays the P-values which are less than or equal to 0.05 (green cells) and the P-values which are greater than 0.05 (purple cells). The variation of correlation coefficients in the spatiotemporal zones is shown in Figure 5-6b. Higher correlation coefficients are at the upper right corner within the first 4 rows and they are also statistically significant. Similar to Figure 5 – 4b, the correlation coefficient values within these spatiotemporal zones (upper right corner) are about 10 times higher than those in other spatiotemporal zones, indicating a possible relationship between antecedent precipitations and total amount of phosphorous within these spatiotemporal zones.

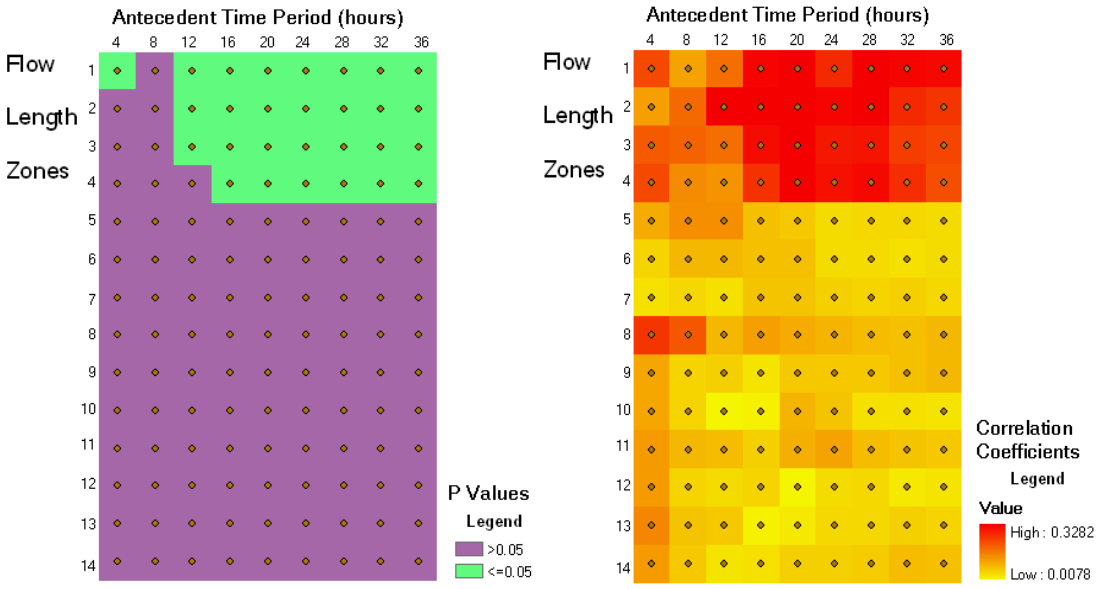

Figure 5-6a & 5-6b. Maps of P-values and correlation coefficients between antecedent precipitations (only with non-zero antecedent precipitations) and total amount of phosphorous for different spatiotemporal zones. The x-axis is antecedent periods (from 4 hours to 36 hours) and y-axis is flow length zones.

The highest coefficient (0.3282) occurred twice in Table 5-5, one comeing from the flow length less than 4.138 km and antecedent period less than 20 hours and the other from the flow length less than 9.867 km and antecedent period less than 12 hours. Among the significant correlation coefficients within the first four flow length zones, antecedent periods between 16 and 36 hours have higher correlation coefficients than others, indicating a

stronger significant statistical relationship between antecedent precipitation and total amount of phosphorous within those antecedent periods, especially within the antecedent period of 20 hours, which has relatively the highest correlation coefficient value. One possible reason to explain this longer antecedent period is that a longer time period has a higher chance of precipitation. Based on these observations, antecedent precipitation which occurs within a shorter flow length (i.e., closer to the water samples) and with a longer antecedent time period might affect water quality more significantly than those that are far away from the samples.

The antecedent period of 20 hours within the first four flow lengths has the highest correlation coefficients except for the 2nd flow length which has the second highest coefficient (0.3026). This indicates that antecedent rainfalls within this time period affect the amount of phosphorous most strongly. Figures 5-7a to 7d show the relationship between antecedent precipitation and the total amount of phosphorous within those spatiotemporal zones. In these figures, we can observe that even for the spatiotemporal zones that have the highest correlation coefficients. However, the relationship between antecedent precipitation and total amount of phosphorous is not as strong.

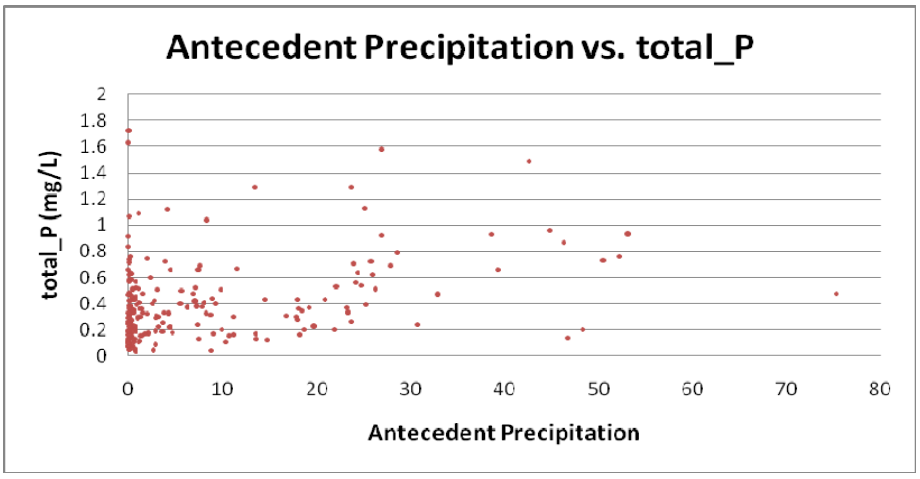

Figure 5-7a. Scatter plot of total amount of phosphorous and antecedent precipitation within the flow length zone of 0 to 4.138 km and antecedent period of 20 hours.

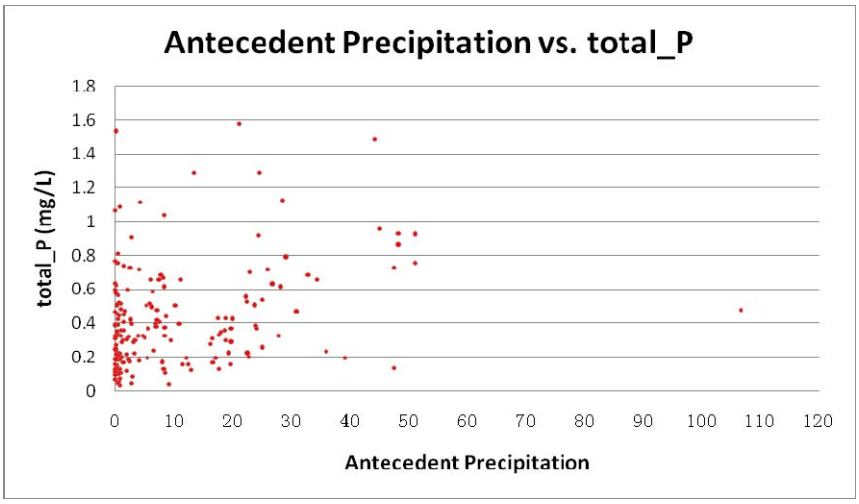

Figure 5-7b. Scatter plot of total amount of phosphorous and antecedent precipitation within the flow length zone of 0 to 9.867 km and antecedent period of 20 hours

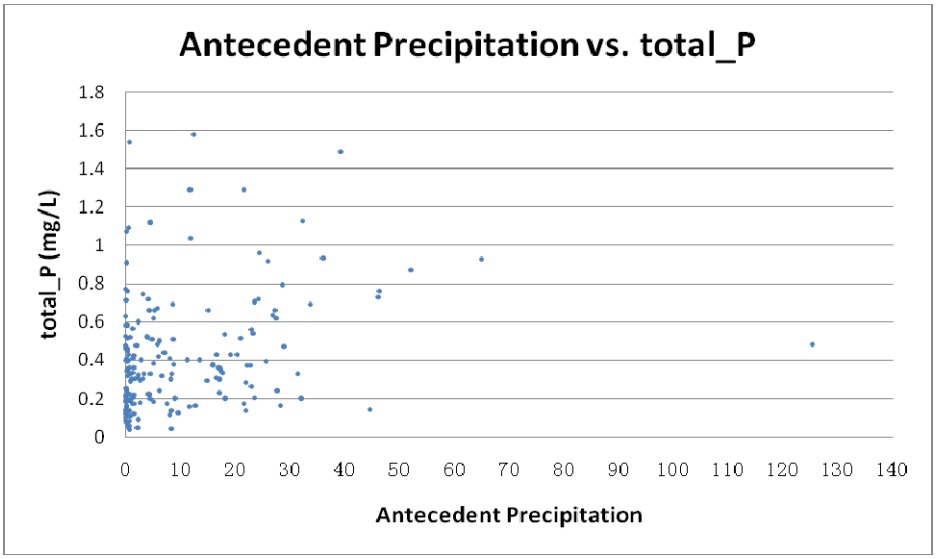

Figure 5-7c. Scatter plot of total amount of phosphorous and antecedent precipitation within the flow length zone of 0 to 21.666 km and antecedent period of 20 hours

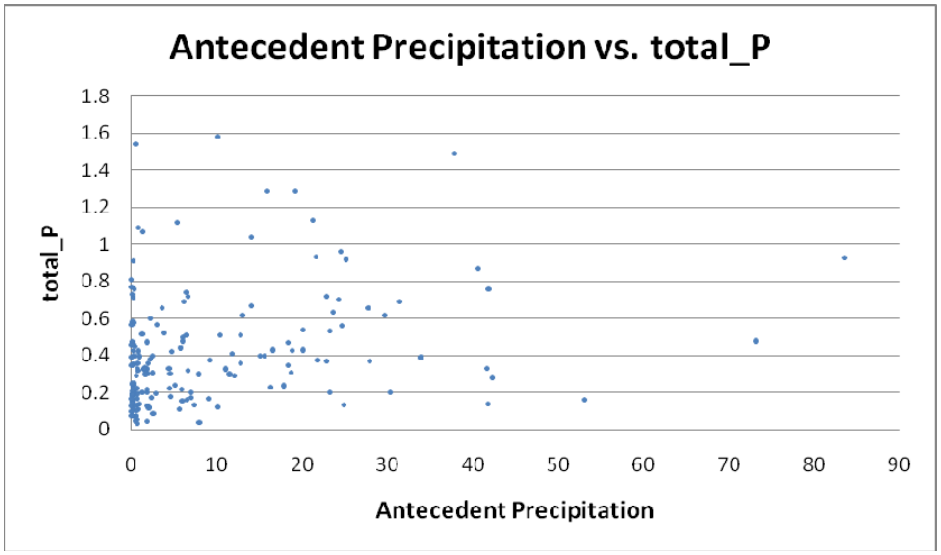

Figure 5-7d. Scatter plot of total amount of phosphorous and antecedent precipitation within the flow length zone of 0 to 40.497 km and antecedent period of 20 hours

5.3.3 Statistical Results for Turbidity

Water turbidity is another water quality measurement that is regularly collected at KBS. Usually, high water turbidity is related to high values of phosphorus. To attempt to verify this, I correlated turbidity with total phosphorus, but the correlation coefficient was only 0.2353. Although the coefficient was low, the p-value was 2.52E-05, which indicates a significant correlation between the two water quality variables. Because of this, I would expect a weak relationship between antecedent precipitation and turbidity as it exists between antecedent precipitation and total phosphorus.

There were 314 unique water samples that have turbidity measurements. I used the same spatiotemporal zones to examine the relationship between antecedent precipitation and turbidity. Table 5–6 shows the correlation coefficients between antecedent precipitation (including zero precipitation) and turbidity of the water samples.

Table 5–6. Correlation coefficients between precipitation and water turbidity for each spatiotemporal zone at?? the water samples. Numbers in the parentheses in the first column are the numbers of water samples. Numbers in the parentheses in the rest of the columns are P values of the coefficient correlations

Time / FL (km)	0-4 hours	0-8 hours	0-12 hours	0-16 hours	0- 20 hours	0-24 hours	0-28 hours	0-32 hours	0-36 hours
0 – 4.138 (314)	0.0358 (0.5263)	0.1215 (0.0313)	0.2212 (7.67E-05)	0.2366 (2.27E-05)	0.2175 (0.0001)	0.2188 (9.26E-05)	0.2243 (6.06E-05)	0.2469 (9.54E-06)	0.2934 (1.18E-07)
0 – 9.867 (314)	0.0368 (0.5148)	0.1175 (0.0372)	0.2153 (0.001)	0.2374 (2.12E-05)	0.2198 (8.54E-05)	0.2203 (8.24E-05)	0.2246 (5.89E-05)	0.243 (1.33E-05)	0.2809 (4.18E-07)
0 – 21.666 (306)	0.0261 (0.6486)	0.0943 (0.1007)	0.193 (0.0006)	0.2063 (0.0002)	0.2012 (0.0003)	0.2008 (0.0004)	0.2037 (0.0003)	0.2205 (0.0001)	0.252 (8.1E-06)
0 – 40.497 (280)	0.0099 (0.868)	0.0715 (0.2324)	0.1558 (0.009)	0.1519 (0.0108)	0.1981 (0.0007)	0.1993 (0.0007)	0.2036 (0.0006)	0.2234 (0.0002)	0.2549 (1.57E-05)
0 – 61.364 (253)	0.0111 (0.8601)	0.0159 (0.8002)	0.066 (0.2973)	0.1166 (0.064)	0.1860 (0.0029)	0.1871 (0.0028)	0.1883 (0.0026)	0.2063 (0.0009)	0.2352 (0.0002)
0 – 92.429 (212)	0.0231 (0.7376)	0.0213 (0.7577)	0.0417 (0.5459)	0.0612 (0.3751)	0.0624 (0.3657)	0.0772 (0.2631)	0.0801 (0.2452)	0.1037 (0.1319)	0.1478 (0.0313)

0 – 138.794 (188)	0.0154 (0.8337)	0.0187 (0.7984)	0.0369 (0.6142)	0.1171 (0.1092)	0.1136 (0.1203)	0.1573 (0.031)	0.1593 (0.0028)	0.1806 (0.0131)	0.2157 (0.0029)
0 – 184.739 (154)	0.0006 (0.9937)	0.0115 (0.8866)	0.0172 (0.8321)	0.0916 (0.2566)	0.0874 (0.2811)	0.1209 (0.1350)	0.1201 (0.1376)	0.1262 (0.1185)	0.1354 (0.0938)
0 – 257.894 (115)	0.0416 (0.6587)	0.0144 (0.8754)	0.0126 (0.8931)	0.0915 (0.3305)	0.0885 (0.3467)	0.0971 (0.3021)	0.0863 (0.359)	0.0864 (0.3581)	0.1011 (0.2825)
0 – 328.024 (90)	0.0701 (0.518)	0.0781 (0.4597)	0.07771 (0.4662)	1.42E-05 (0.9998)	0.0387 (0.7171)	0.0365 (0.7321)	0.0302 (0.7772)	0.0292 (0.7841)	0.0423 (0.6917)
0 – 430.00 (72)	0.0798 (0.5048)	0.0829 (0.4884)	0.0799 (0.5041)	0.0189 (0.8745)	0.146 (0.2208)	0.1232 (0.3025)	0.1225 (0.3051)	0.1178 (0.324)	0.1189 (0.3194)
0 – 530.00 (72)	0.0688 (0.5656)	0.0778 (0.5157)	0.0676 (0.5722)	0.0478 (0.6901)	0.1196 (0.3168)	0.1234 (0.3017)	0.1236 (0.3007)	0.1182 (0.3227)	0.1205 (0.3131)
0 – 630.955 (72)	0.0511 (0.6698)	0.0826 (0.4898)	0.0739 (0.5371)	0.0558 (0.6409)	0.0417 (0.7276)	0.0677 (0.5715)	0.0692 (0.5632)	0.0688 (0.5654)	0.0818 (0.4944)
0 – 972.235 (72)	0.0634 (0.5967)	0.0028 (0.9809)	0.0119 (0.9209)	0.0223 (0.8521)	0.0197 (0.8692)	0.1929 (0.1043)	0.2063 (0.0819)	0.2056 (0.0831)	0.208 (0.0795)

Correlation coefficients in the table 5-6 are low [say something about how they compare to the earlier analysis]. The highest correlation coefficient in table 5-6 is 0.2934. It is located within the first flow length zone and an antecedent period of 36 hours. P-values and correlation coefficients maps are shown in Figure 5-8a and 5-8b. Seventy percent of the P-values are higher than 0.05 and only a few within the first 5 flow length zones and the seventh flow length zone are lower than 0.05, indicating a possible significant relationship between antecedent precipitation and turbidity in those spatiotemporal zones. As flow length increases, only longer antecedent time periods have P-values less than 0.05. In the correlation coefficient map, higher correlation coefficients (red cells in Figure 5-8b) are located within the spatiotemporal zones where their P-values are also less than 0.05 (green cells in Figure 5-8a). Some higher correlation coefficients are located at the longest flow length zone within antecedent periods from 24 to 36 hours. However, the P-values in those spatiotemporal zones are higher than 0.05, indicating no significant statistical relationships in those zones and this might be caused by sample size problems. In addition, for these significant correlation coefficients, within each antecedent time period, they decrease as flow length increases. On the other hand, within each flow length zone, these significant correlation coefficients increase when antecedent period increases. Thus, these results imply that precipitation closer to the water sample locations and within a longer antecedent period affect water turbidity more strongly.

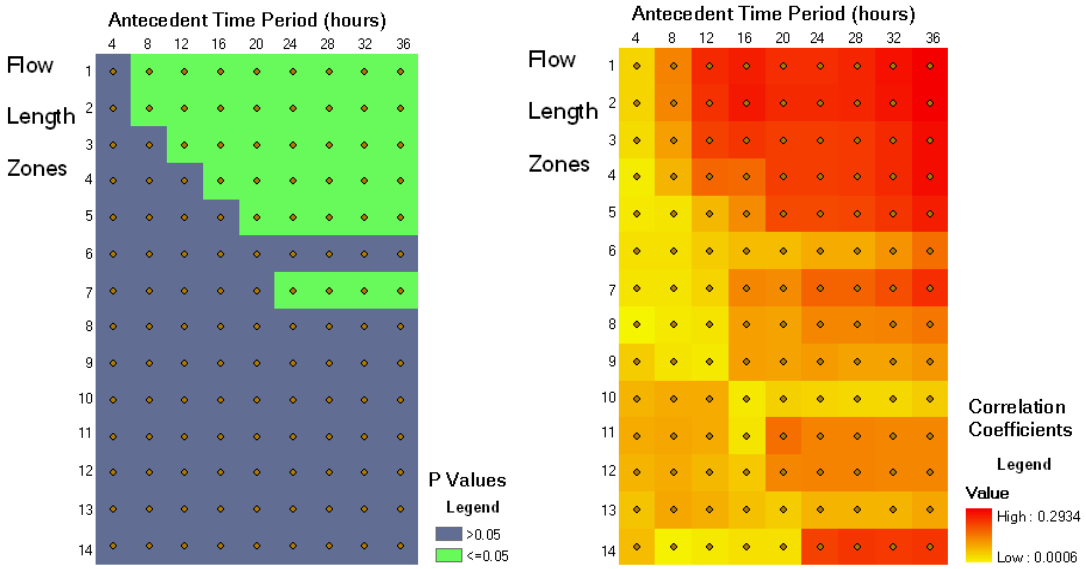

Figure 5-8a & 5-8b. Maps of P-values and correlation coefficients between antecedent precipitation (including zero antecedent precipitations) and water turbidity for different spatiotemporal zones. The x-axis is antecedent periods (from 4 hours to 36 hours) and y-axis is flow length zones.

Table 5-7 shows the correlation coefficients between non-zero antecedent precipitation and turbidity. It only contains the coefficients for the first five flow length zones, because the P-values for all other correlation coefficients are higher than 0.05. Furthermore, some of the spatiotemporal zones don't have sufficient samples (less than 30) for statistical analysis.

The following table gives us similar information as seen in Table 5-5. The correlation coefficients are relatively higher than those calculated using all antecedent precipitation (including zero precipitation). However, the coefficients are still low and don't indicate a good relationship between antecedent precipitation and water turbidity. The highest coefficient is 0.3587 and is found within the flow length less than 4.138 km and antecedent period of 36 hours.

Table 5-7. Correlation coefficients between non-zero antecedent precipitation and water turbidity for the combinations of flow length and antecedent time. The first number in the parenthesis is the number of water samples and the second number in the parenthesis is the p-value of the correlation coefficient.

Time / FL (km)	0-4 hours	0-8 hours	0-12 hours	0-16 hours	0- 20 hours	0-24 hours	0-28 hours	0-32 hours	0-36 hours
0 – 4.138	0.0642 (36,0.7098)	0.2194 (45,0.1475)	0.2898 (63,0.0212)	0.3106 (65,0.0117)	0.2781 (65,0.0248)	0.288 (89,0.0062)	0.2972 (89,0.046)	0.2856 (106,0.0029)	0.3587 (108,0.0001)
0 – 9.867	0.1462 (30,0.4578)	0.2618 (34,0.1346)	0.2815 (54,0.0391)	0.3106 (55,0.0209)	0.2856 (55,0.0344)	0.3292 (79,0.0031)	0.3372 (79,0.0023)	0.2745 (100,0.0057)	0.3205 (103,0.0009)
0 – 21.666	0.0435 (34,0.8067)	0.163 (40,0.3149)	0.2351 (57,0.0782)	0.242 (58,0.0671)	0.2481 (59,0.058)	0.2929 (75,0.0107)	0.2982 (75,0.0093)	0.2401 (96,0.0184)	0.2820 (97,0.0051)
0 – 40.497	0.0137 (35,0.9374)	0.1225 (42,0.4392)	0.1964 (56,0.1467)	0.1815 (57,0.1766)	0.2771 (57,0.0352)	0.2565 (73,0.0284)	0.2638 (73,0.0241)	0.2266 (92,0.0298)	0.266 (93,0.0095)
0 – 61.364	0.1168 (31,0.5312)	0.0218 (38,0.8965)	0.0205 (53,0.8836)	0.1298 (55,0.3448)	0.2835 (55,0.0358)	0.2687 (69,0.0255)	0.2705 (69,0.0245)	0.2253 (63,0.0369)	0.2656 (88,0.0123)

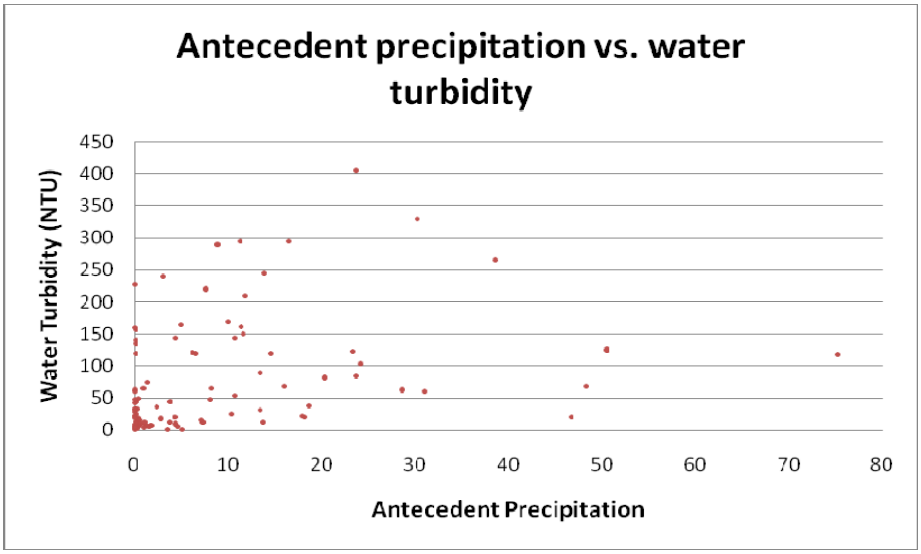

Figure 5-9. Antecedent precipitation and water turbidity within the spatiotemporal zone which has the highest correlation coefficient

Figure 5-9 is a scatter plot of antecedent precipitation and water turbidity in the spatiotemporal zone which has the highest correlation coefficient. 65% of the turbidity values of the water samples are less than 50 NTU and are associated with nearly zero antecedent precipitation. We can roughly see that when antecedent precipitation increases, turbidity also increases. With a P-value of 0.0001 and correlation coefficient of 0.3587, there is a statistical relationship between antecedent precipitation and turbidity within the first flow length zone and antecedent period of 36 hours. However, it is not a strong relationship and is not obvious from the figure.

Generally speaking, for the statistically significant correlation coefficients in the above tables, the correlation coefficients decrease as flow length increases, and within each flow length zone, the correlation coefficients increase when the antecedent period increases. This indicates that longer antecedent periods and precipitation near to the water sample locations affects water quality (turbidity and total amount of phosphorus) more than the antecedent precipitation in longer flow length and shorter antecedent time periods spatiotemporal zones.

5.4 Procedures to Perform the Spatiotemporal Analysis

In order to help other researchers perform the above analysis with their own water samples, flow lengths, and antecedent periods, detailed steps involved in the analysis are described in this section. The data needed in the analysis include water sample data saved as an ESRI point shapefile and a Digital Elevation Model (DEM), which is used to derive flow direction and flow accumulation raster layers. The first step is to check the coordinate systems of the data to make sure that all of them are in the Hydrologic Rainfall Analysis Projection (HRAP) coordinate system used in the NEXRAD precipitation database. If they are not, they should be projected into HRAP by using the NexTool software discussed in section 4.3. With the DEM and water sample points as outlets, flow direction and the watershed associated with each water sample can be delineated using the hydrological function available in ArcGIS. With the flow direction in each watershed, flow length can then be calculated by using the FlowLength function in ArcGIS. The figure below shows what a flow length raster layer looks like.

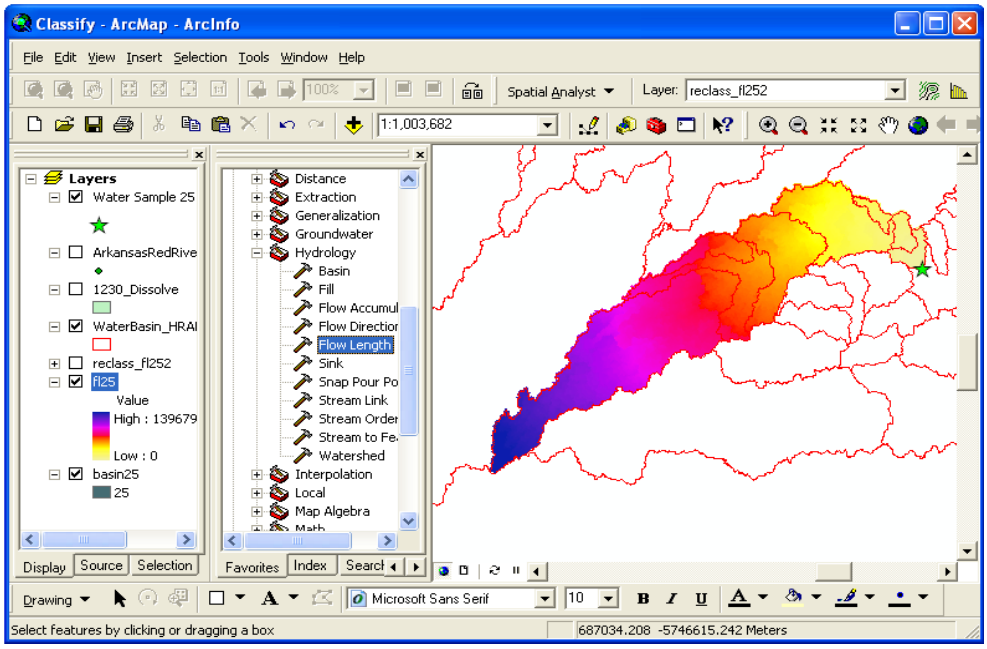

Figure 5-10. Flow length for a water sample.

The next step is to divide a watershed into several spatial zones based on the flow length in the watershed. The number of zones and the threshold values used to define the zones are application dependent and should be based on the potential effects of flow length on water quality. The Reclassify function in ArcGIS can be used to generate the zones. The following figure shows the result after the watershed associated with a water sample is classified into 7 flow length zones.

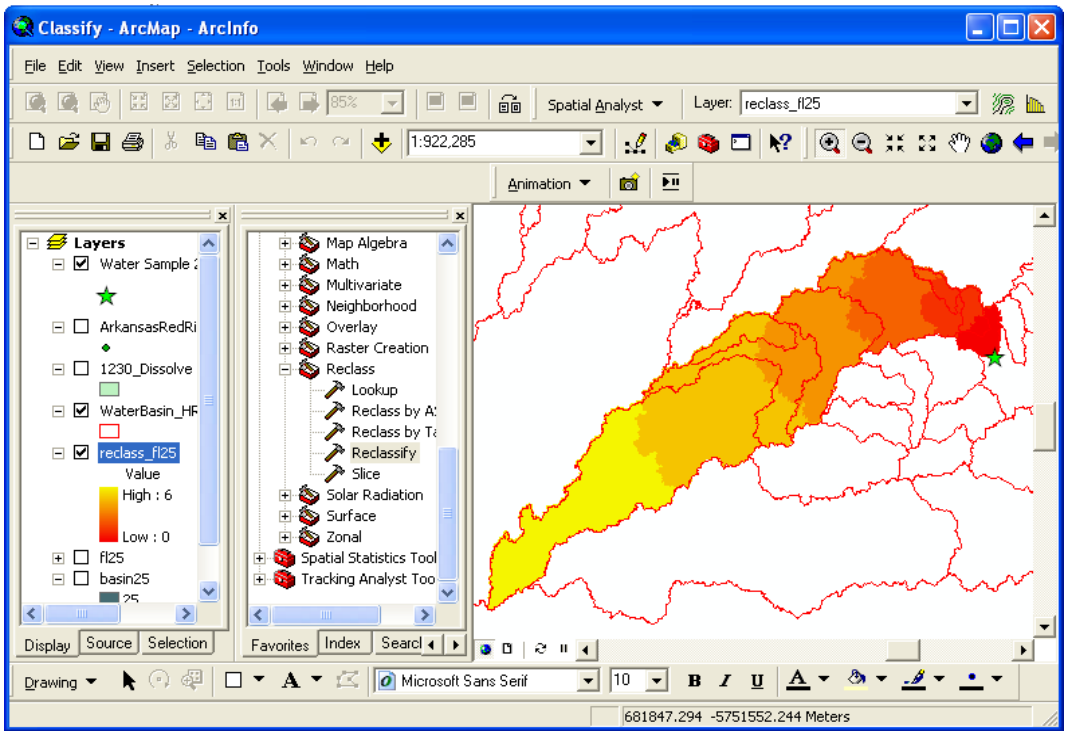

Figure 5-11. Classification of watersheds into flow length zones.

After reclassification, we need to convert the flow length raster zones into a polygon shapefile, which is the required input data format for the NexTool software. This raster-to-vector conversion usually creates many small polygons, each of which has a unique ID. We need to combine those small polygons if they are from the same raster zones. This can be done by using the Dissolve function available in ArcGIS. The following figure shows the polygon flow length zones after raster-to-vector conversion and applying the dissolving function (Figure 5-12).

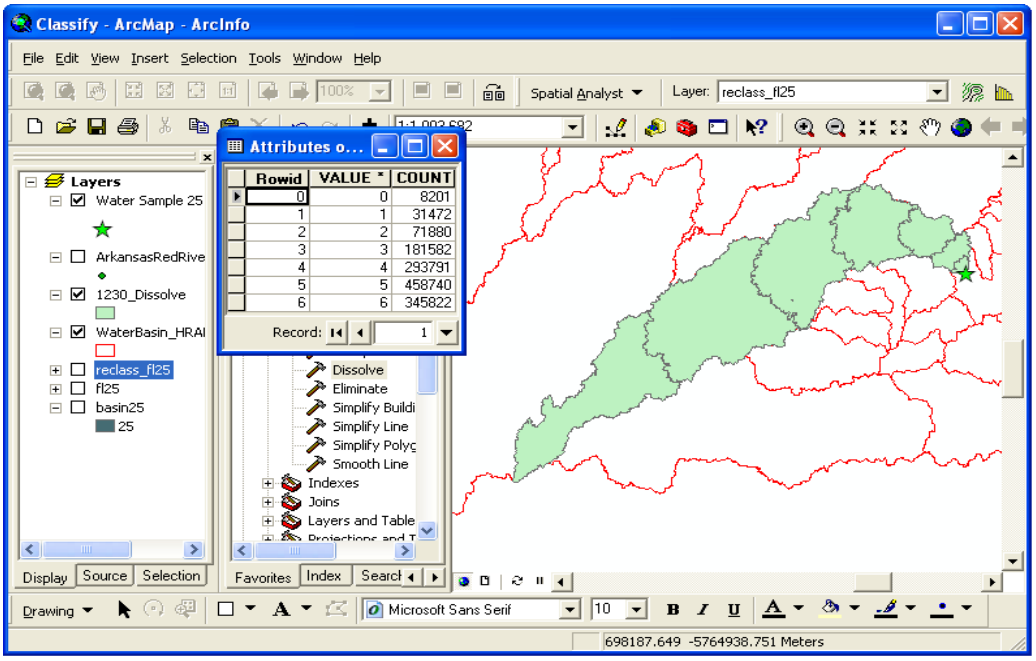

Figure 5-12. Vector flow length zones for the watershed associated with the water sample in Figure 5-11.

Now we are done with the analysis in GIS and we have a polygon shapefile which stores flow length zones. We next use the NexTool software, which was introduced in chapter 4. We extract antecedent precipitation from spatiotemporal zones by using the weighted area method discussed in section 4.5. First, we need to calculate areal weights associated with each flow length zone. Figure 5-13 shows the user interface for calculating the weights.

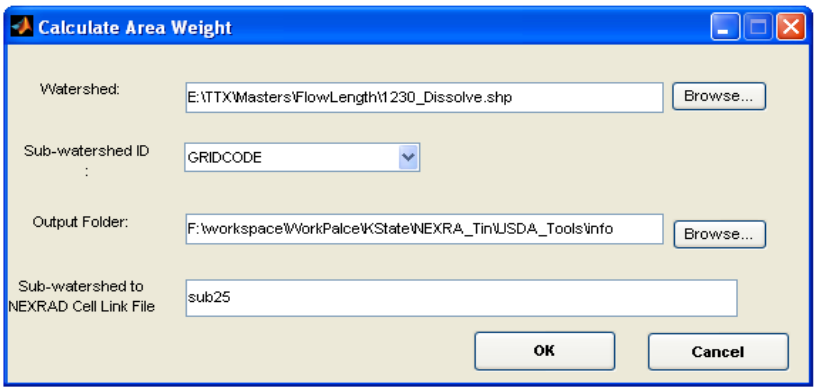

Figure 5-13. User interface in the NexTool to calculate areal weights for each flow length zone.

The result from this tool is a text file (Figure 5-14) which stores the relationship between each flow length zone and the NEXRAD cells which intersect with the flow length zone. Each row in the file contains the flow length zone ID, NEXRAD cell ID, the percentage of area of the NEXRAD cell covered by the flow length zone, and several other pieces of useful values.

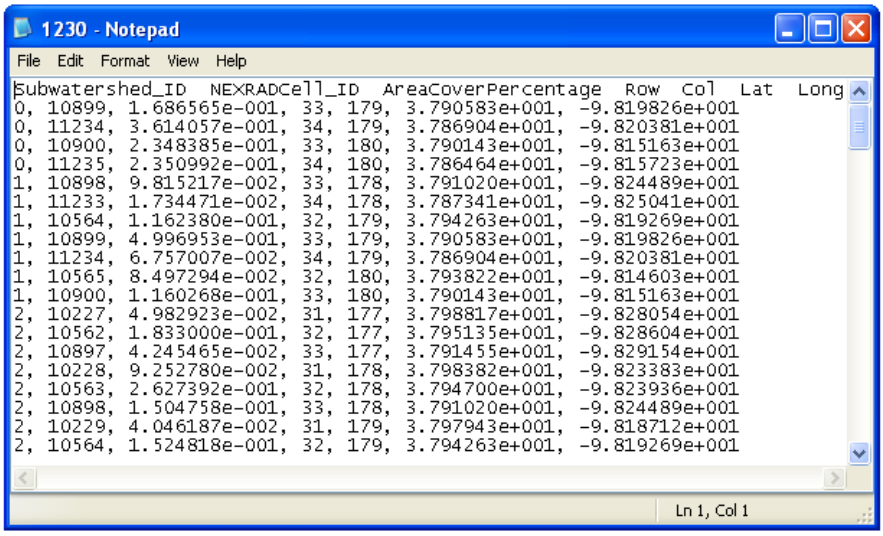

Figure 5-14. Output text file from the NexTool software. The text file stores the areal weights for each flow length zone.

The areal weight text file is then used to extract antecedent precipitation with the following user interface in the NexTool (Figure 5-15).

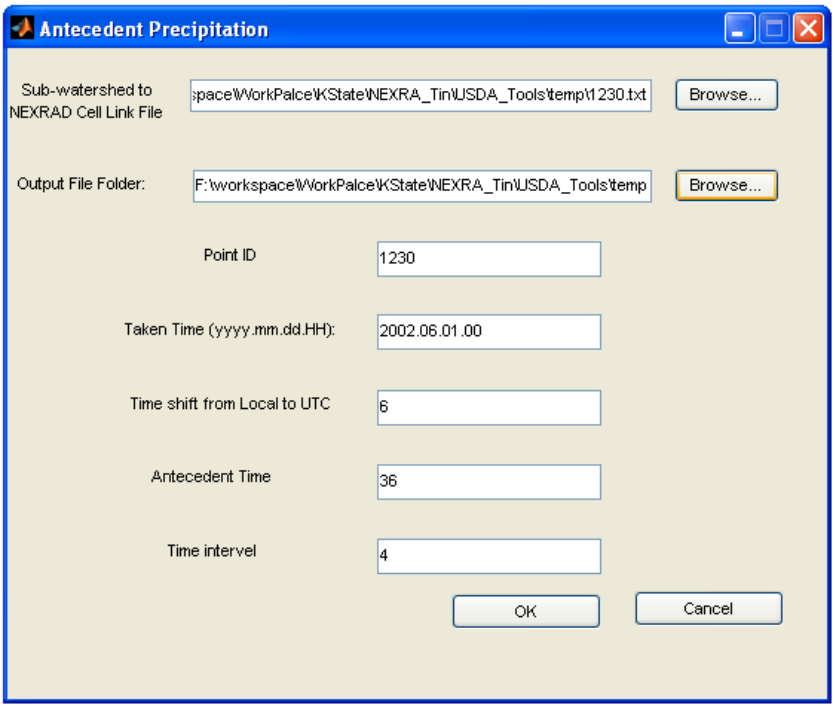

Figure 5-15. User interface in NexTool to extract antecedent precipitation.

The linked file on the user interface is the text file which stores the areal weights for each flow length zone. Point ID is the ID of a water sample for which antecedent precipitation in different spatiotemporal zones will be extracted. Taken Time is the date and time when the water sample was collected. Several water samples might be taken at the same location but at different times. Since most of the water samples didn't record the exact time when the sample was collected, we used time around 12:00 pm as the default data collection hour. Time shift Local to UTC indicates the difference between UTC time and local time as the NEXRAD precipitation database is based on the UTC time. Antecedent time on the interface decides the antecedent period to extract precipitation and the Time interval item determines the number of temporal zones. For example, if the antecedent time is set to 36 hours and time interval is set to 4, there would be 9 temporal zones for each flow length zone. The combination of spatial flow length zones and temporal zones creates spatiotemporal zones. This tool generates a text file which records cumulative antecedent precipitation within each spatiotemporal zone (Figure 5 – 16). The

antecedent precipitation can then be used for further statistical analysis. For the example water sample in Figure 5-12, since it has 7 flow length zones and each flow length zone has 9 antecedent periods, there are a total of 63 antecedent precipitation values extracted for the water sample.

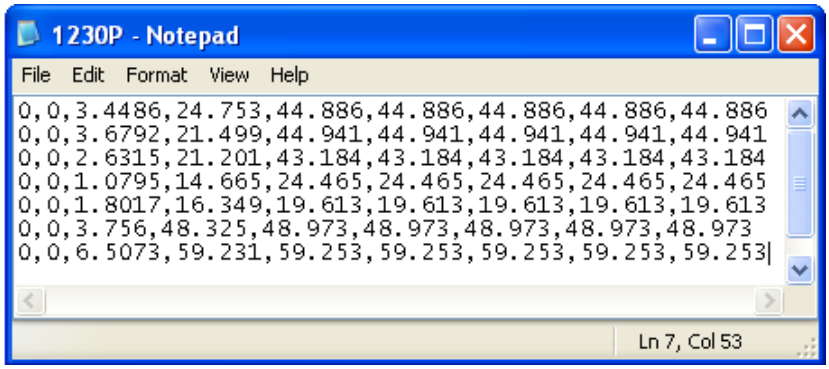

Figure 5-16. Cumulative antecedent precipitation within 63 spatiotemporal zones.

Chapter 6. Conclusions and Future Researches

6.1 Conclusions

This research extends the cartographic modeling operations to analyze spatiotemporal datasets. More specifically, it developed zonal operations to handle vector spatiotemporal zones, which are lacking in current GIS implementations. Those zonal operations were tested and used in two applications, one for the generation of precipitation input for non-point source pollution models and the other for exploring the effect of antecedent precipitation on water quality.

Current cartographic modeling operations only work with raster layers, which are measured at a particular moment or during a certain period of time. Because of the lack of a temporal dimension, only spatial analysis can be performed on the raster layers. In addition, some geographic phenomena are better represented as vector features rather than raster layers and there is no corresponding operation available in the vector data model. With the increasing availability of spatiotemporal data and the demand for spatiotemporal analysis, this research extended the original zonal functions to handle spatiotemporal data with vector zones.

A software package, NexTool, was developed to use NEXRAD precipitation data. The software provides the functions to build spatiotemporal precipitation databases, to convert between different coordinate systems, and to visualize precipitation databases. An hourly NEXRAD precipitation database, which covers the ABRFC and covering 11 years (from October 1, 1995 to September 30, 2006), was created using the software.

The vector zonal operation and the NEXRAD precipitation database were first used to generate daily precipitation input for non-point source pollution models (AnnAGNPS and SWAT). Daily precipitation within vector spatiotemporal zones was extracted from the NEXRAD precipitation database. In this case, sub-watershed boundaries used in the models defined the spatial extent of the spatiotemporal zones and a day (i.e., 24 hours)

defined the temporal extent of the spatiotemporal zones. The area-weighted vector zonal summary operation was used to calculate daily total precipitation within each sub-watershed.

The vector zonal summary operation was also used to explore the effects of antecedent precipitation on water quality. Precipitation that occurred within a certain number of hours before a water sample was taken and was within a certain flow length was extracted from the NEXRAD precipitation database. In this case, sub-watershed flow length defined the spatial extent of a spatiotemporal zone and antecedent period defined the temporal extent of the spatiotemporal zone. Different flow lengths and antecedent periods were used to identify the spatiotemporal zones in which precipitation might affect water quality. Based on the analysis in chapter 5, significant correlation coefficients occurred only for flow lengthes less than 40.49 km. Those significant correlation coefficients generally decreased as flow length increased and they increased as antecedent periods increased. A preliminary conclusion from this analysis is that antecedent precipitation which occurred 12 to 36 hours before a water sample was collected and within 40 km of flow length from the water sample location affected the turbidity and total amount of phosphorus the most.

6.2 Future Researches

Although this research discussed the general concept of vector cartographic modeling operations for spatiotemporal analysis, it focused only on one such operation (i.e., spatiotemporal zonal summary). In a future study I plan to explore other vector cartographic operations, including local and focal operations, for spatiotemporal analysis. In addition, although this research discussed three types of spatiotemporal zones based on the work from Mennis (2005), it does not discuss how spatiotemporal zones can be defined efficiently and precisely for specific applications. While defining spatial zones

has matured and been implemented in many GIS software packages, defining temporal zone efficiently need further research.

The NexTool is a powerful software tool to handle NEXRDA data but it has some limitations. First, the software is based on MATLAB and thus requires a MATLAB runtime application installed in order to use the tool. Second, the software tool only provides the coordinate system conversion between NAD83 and HRAP, which are often used for hydrological analysis. Third, the software can only generate daily precipitation inputs for two non-point source pollution models (AnnAGNPS and SWAT). New functions must be added in order to generate precipitation inputs for other models. The software needs to be further developed to overcome these limitations.

One issue in exploring the effects of antecedent precipitation on water quality is how to more objectively select flow length thresholds. There is a big gap between two set of flow lengths, from thousands of meters to millions of meters. I chose the flow lengths subjectively. As such, if the number of flow length zones is too small, some critical flow lengths might be missed. Because of this, this thesis provided detailed steps to perform the analysis so that other researchers can follow the steps if they want to use their own spatiotemporal zones. Many other methods could be applied to make flow length threshold values for different analysis purposes, such as Jenks optimal method of data classification within ArcGIS.

Another issue I noticed was that from all the correlation coefficients tables, most of the correlation coefficients increased as antecedent time period increased and researched the highest value at 0 to 36 antecedent time period. No longer antecedent time period than 36 hours was test because this is the longest time which would affect water quality by conclusions of the experts of KBS. But now we may doubt the longest antecedent time period. Because there is no result for 0-40 antecedent time period, will the correlation coefficients still increase in that time period or will they decrease. Only when we know

the correlation coefficients result from longer time periods than 0 to 36 hours, we can conclude what is the longest antecedent time that within which the precipitation will still affect water quality.

Finally, water quality is not just affected byprecipitationl. The low correlation coefficients between antecedent precipitation and water quality measurements indicated this. Many other factors, such as land use, soil type, and temperature, may also affect water quality. This research simply assumes that other conditions for the entire Arkansas Red River Basin are uniform. To better understand the effect of precipitation on water quality, many other environmental factors, such as land use type, soil erosion and etc., should be considered in the future.

Acknowledgements

This research was partially supported by the United States Department of Agriculture under grant FED38300.

References

AnnAGNPS: Annualized Agricultural Nonpoint Source Pollution Model, U.S. Department of Agriculture, http://msa.ars.usda.gov/ms/oxford/nsl/AGNPS.html

ArcGIS Desktop 9.2 Help. 2007. How to delineate watershed, ESRI, http://webhelp.esri.com/arcgisdesktop/9.2/index.cfm?TopicName=Delineating_watersheds

Buttner, J. K., Soderberg, R. W., Terlizzi, D. E. 1993. *An Introduction to Water Chemistry in Freshwater Aquaculture*, NRAC Fact Sheet No. 170-1993

Ciach, G.J. and Krajewski, W.F. 1999. Radar-rain gauge comparisons under observational uncertainties. *Journal of Applied Meteorology*,38: 1519-1525.

Dalton, Jason. 2005. Temporal Analysis and GIS, Geospatial Solutions, http://www.geospatial-solutions.com/geospatialsolutions/Main+Feature/Temporal-Analysis-and-GIS/ArticleStandard/Article/detail/153302

David I. Stern. 2005. *A Three-Layer Atmosphere-Ocean Time Series Model of Global Climate Change.* Rensselaer Working Papers in Economics 0510, Department of Economics, Rensselaer Polytechnic Institute, NY.

Egenhofer, M.J. and Herring, J. 1991. *Categorizing binary topological relationships between regions, lines, and points in geographic databases.* Technical Report, Department of Surveying Engineering, University of Maine, Orono, ME.

\French, K. and X. Li (in press). Feature-based cartographic modeling, *International Journal of Geographic Information Science*.

Fulton, R.A. 2002. *Activities to improve WSR-88D radar rainfall estimation in the National Weather Service*, 2nd Federal Interagency Hydrologic Modeling Conference, Las Vegas, Nevada, July 28-August 1.

Fulton, R.A., Breidenbach, J.P., Seo, D., Miller, D.A., and O'Bannon, T. 1998. The WSR-88D rainfall algorithm, *Weather and forecasting* 13: 377-395.

Fulton, R.A., F. Ding and D.A. Miller. 1998. *Truncation Errors in Historical WSR-88D Rainfall Products.* Conference on Radar Meteorology, Seattle, Washington.

Garbrecht, J., Ogden, F.L., Debarry, P.A., Maidment, D.R. 2001. GIS and distributed watershed models I: data coverages and sources. *Journal of Hydrologic Engineering* 6: 506-514.

Greene, D.R., Hudlow, M.D. 1982. *Hydrometeorologic grid mapping procedures.* In: American Water Resources Association International Symposium on Hydrometeorology, Herndon, USA, 55-68.

Jackson, T. J., Le Vine, D. M., Griffis, A. J., Goodrich, D. C., Schmugge, T. J., Swift, C. T., O'Neill, P. E. 1993. Soil moisture and rainfall estimation over a semiarid environment with the ESTAR microwave radiometer. *IEEE Transactions on Geoscience and Remote Sensing* 31(4): 836-841

Krajeski, W.F. and Smith, J.A. 2002. Radar hydrology: Rainfall estimation, *Advances in Water Resources* 25: 1387-1394.

Krajewski, W.F. 1987. Co-kriging of radar rainfall and rain-gauge data, *J. geography research* 92: 9571-9580.

Krajewski, W. F., G. J. Ciach, and E. Habib, 2003. An Analysis of Small-Scale Rainfall Variablity in Different Climate Regimes. *Hydrologic Sciences Journal* 48: 151-162.

Klazura, G.E. and D.A. Imy. 1993. A description of the initial set of analysis products available from the NEXRAD WSR-88D system, *Bull. Amer. Meteor. Soc* 74: 1293-1311.

Ledoux, H. and Gold, C. 2006. A Voronoi-based map algebra. *Progress in Spatial Data Handling-12th International Symposium on Spatial Data Handling*: 117-131.

Longley, P. A., M. F. Goodchild, D. J. Maguire, and D. W. Rhind. 2001. *Geographic Information Systems*. Chichester: John Wiley and Sons.

Li, Xingong. and Hodgson, M.E. 2004. Vector field data model and operations. *GIScience and Remote Sensing* 41(1): 1-24.

Martinko, E., J. Whistler, D. Peterson, J. Kastens, R. Hagen, D. Huggins, M. Jakubauskas. 2007. *A Watershed Classification System for Tiered Diagnosis of Biological Impairments: A Scalable, Central Plains Focus with National Applicability.* KBS report 141, Kansas Biology Survey, University of Kansas, Lawrence, 153pp.

Mennis, J. 2003. Derivation and implementation of a semantic GIS data model informed by principle of cognition. *Computer, Environment, and Urban Syatems* 27: 455-79

Mennis, J., and D. J. Peuquet. 2003. The role of knowledge representation in geographic knowledge discovery: A case study. *Transactions in GIS* 7: 371-91

Mennis, J., Viger, R., and Tomlin, D. 2005. Cubic map algebra functions for spatiotemporal analysis. *Cartography and Geographic Information Science* 32(1): 17- 32.

Nathalie Pettorelli, Jon Olav Vik, Atle Mysterud, Jean-Michel Gaillard, Compton J. Tucker, Nils Chr. Stenseth. 2005. Using the satellite-derived NDVI to assess ecological responses to environmental change, *Trends in Ecology & Evolution* 20 (9): 503-510

Nadi, S., Delavar, M. R. 2001. *Spatio-Temporal Modeling of Dynamic Phenomena in GIS.* Department of Surveying and Geomatic Eng., University of Tehram.

Neitsch, S.L., Arnold, J.G., Kiniry, J.R., Williams, J.R., King, K.W. (2002). *Soil Water Assessment Tool Theoretical Documentation,* http://www.brc.tamus.edu/swat/downloads/doc/swat2000theory.pdf

Nelson, B.R., Krajewski, W.F., Kruger, A., Smith, J.A., Baeck, M.L. 2003. Archicval precipitation data set for the MIissippi River Basin: development of a GIS-based data brower. *Computers and Geosciences* 29 (5): 595-604.

NOAA, NEXRAD Stage III Precipitation Data, 2002
http://www.nws.noaa.gov/oh/hrl/dmip/nexrad.html

NWS, Provision of NWS Information in Geospatial Format,,2007
https://ocwws.weather.gov/gis/index.php

NWS, Arkansa Red-River Basin River Forecast Center, 2007
http://www.srh.noaa.gov/abrfc/index.htm

NWS Office of Hydrology. 1997. *Stage III precipitation processing system guide*, Hydrologic Research Laboratory,

Ogden, F.L., Garbrecht, J.F.L., Debarry, P.A., Maidment, D.R. 2001. GIS and distributed watershed models II: modules, interfaces, and models. *Journal of Hydrologic Engineering* 6: 515-523.

Reed, S.M. and Maidment, D.R. 1999. Coordinate transformation for using NEXRAD data in GIS-based hydrologic modeling, *Journal of Hydrologic Engineering:* 174-182.

Salamanca, E. F., Nobuhiro Kaneko, and Shigeo Katagiri. 2002. Rainfall manipulation effects litter decomposition and the microbial biomass of the forest floor, *Applied Soil Ecology* 22(3): 271-281

Scoot, M. 1999. *The extension of cartographic modeling for volumetric geographic analysis.*
http://www.spatial.maine.edu/~onsrud/ucgis/testproc/scott_m/scottm.html

Tachizuka, S., Hung, T., Ochi, S., and Yasuoka, Y. 2003. *Monitoring of long-term urban expansion by the use of Remote Sensing images from different sensors.* Proc., 23rd Asian Conf. on R.S., Kathmandu, Nepal.
http://www.gisdevelopment.net/aars/acrs/2002/urb/213.pdf

Tang J., Wang L.and Yao Z. 2007. Spatio-temporal urban landscape change analysis using Markov chain model and a modified genetic algorithm, *International Journal of Remote Sensing* 28(15): 3255-3271.

The Mathworks, MatLab Public Website, 2007
http://www.mathworks.com/products/matlab/

Tomlin, C.D. 1990. *Geographic information systems and cartographic modeling*. Englewood Cliffs, New Jersey: Prentice Hall.

Tobler, W. 1995. The resel-based GIS. *International Journal of Geographical Information Systems* 9(1): 95-100.

Turner, M. G. 2007. Spatial and temporal analysis of landscape patterns, *Landscape Ecology* 4(1).

USDA, Revised Universal Soil Loss Equation 2, 2007
http://www.ars.usda.gov/Research/docs.htm?docid=6010

U.S. EPA. 1986, Quality Criteria for Water, EPA 440/5-86-001.

Wang, X. and Pullar, D. 2005, Describing dynamic modeling for landscapes with vector map algebra in GIS. *Computers & Geosciences*, 31(8): 956-967.

Xie, H., X. Zhou, E.R. Vivoni, J.M.H. Henderinkk, E.E. Small. 2005. GIS Based NEXRAD Precipitation Database: Automated Approaches for Data Processing and Visualization. *Computers and Geosciences* 31: 65-76.

University of Washington. 2004. "Hydrologic Modeling and Watershed Delineation", University of Washington
http://courses.washington.edu/esrm590/lessons/hydrology/index.html

Yuan, M. 1996. Temporal GIS and Spatio-Temporal Modeling. NCGIA.

Yuan, M. 2001. Representing Complex Geographic Phenomena in GIS, *Cartography and Geographic Information Science* 28(2): 83-96.

Young, C.B., Nelson, B. R., Bradley, A.A., Krajewski, W.F., Kruger, A., Morissey, M.L. 2000. Evaluating NEXRAD multisensor precipitation estimates for operational hydrolohic forecasting, *Journal of Hydrometeorology* 1: 241-254.

Appendix A

AnnAGNPS (US Department of Agriculture)

AnnAGNPS is a distributed parameter, watershed scale model that is used for continuous simulations and the AnnAGNPS stands forAnnualized Agricultural Nonpoint Source Pollution Model. It is a continuous simulation watershed-scale program developed based on the single-event model AGNPS. AnnAGNPS simulates quantities of surface water, sediment, nutrients, and pesticides leaving the land areas and their subsequent travel through the watershed. Output of the model is expressed on an event basis for selected stream reaches and as source accounting (contribution to outlet) from land or reach components over the simulation period.

AnnAGNPS divides the watershed into homogenous drainage areas, which are then integrated together by simulated rivers and streams, routing the runoff and pollutants from each area downstream. The hydrology of the model is based on simple water balance approach. Inputs of the model are watershed delineation, daily precipitation, temperatures, management information and so on. For the model itself, daily precipitation can be generated by the climate data generator (GEM), which is calculated the daily precipitation by using nearby rain gauges. For my study, instead of using rain gauges, I generated daily precipitation from hourly NEXRAD precipitation database by using Nextool. And after evaluating the NEXRAD daily precipitation input file by comparing it with real rain gauges daily precipitation input file, the NEXRAD daily precipitation input file is more accurate and suitable to use for the Chenny Lake watershed within ABRFC.

Appendix B

SWAT (Neitsch et al., 2002)

SWAT (Soil Water Assessment Tool) is a continuous time nonpoint source modeling that operates on a daily time step at basin scale and can be considered as a watershed hydrological transport model which can handle almost hydrolyogocal analysis such as surface runoff, transmission losses, water transfer, nutrient and pesticide loading, and so on. The objective of this model is to predict the long-term impacts in large basins of management and also timing of agricultural practices within a year. It can be used to simulate at the basin scale water and nutrients cycle in landscapes whose dominant land use is agriculture. It can also help in assessing the environmental efficiency of BMP's (Best Menagement Practice) and alternative management policies.

As AnnANGPS, daily precipitation is a critical input for SWAT ((Neitsch et al., 2002) and the most frequently used daily precipitation data are from rain gauge estimations. In chapter 4, I developed a area weighted method which allowed us to generate daily precipitation input file for SWAT by using NEXRAD hourly precipitation database and Nextool. Testfiy working has been done by people in Kansa State University. They compared the daily precipitation input file for SWAT from both rain gauges and NEXRAD on Chenny Lake watershed and found out the NEXRAD daily precipitation input file can be used to take place of the rain gauge precipitation data.